thetic and vagal nerve activities.

The existence of an accentuated antagonism in the direct action of ACh through the K_{ACh} channels could be explained by macromolecular signaling complexes in which G protein-gated inwardly rectifying potassium (GIRK) channels are physically associated with signaling partner regulated by different G protein-coupled receptors (GPCRs) [19, 20]. Cardiac sympathetic stimulation simultaneously activates several different GPCRs: α-adrenergic, β1-adrenergic, and β2-adrenergic receptors. Notably, the β1-adrenergic receptor is coupled to downstream kinase, protein kinase A (PKA). The β-adrenergic signaling via PKA phosphorylation increases the activity of K_{ACh} channels [21, 22]. Taken together, β-adrenergic receptors might augment the activity of K_{ACh} channels via a PKA-dependent mechanism.

Limitations

This study has several limitations. First, the data was obtained from anesthetized animals. Since anesthesia would affect the autonomic tone, the results may not be directly applicable to conscious animals. However, because we cut and stimulated the right cardiac sympathetic and vagal nerves, changes in autonomic outflow associated with anesthesia might not have significantly affected the present results.

Second, we blocked the K_{ACh} channels to examine the effect of background sympathetic tone on the direct effect of ACh through the K_{ACh} channels. On the other hand, if we had blocked the indirect effect of ACh through the cyclic AMP pathway, leaving the direct effect of ACh intact, and then examined the effect of background sympathetic tone on the HR response to vagal stimulation, the results might have been excessively straightforward. However, we could find no blocker for the indirect effect of ACh alone that was suitable for in vivo study at present. Further studies are required to directly examine the effect of background sympathetic tone on the direct effect of ACh through the K_{ACh} channels.

In conclusion, concomitant CSS affected no parameters of rapidity (i.e., the corner frequency in the frequency domain and the time constant in the time domain) of vagal HR control via K_{ACh} channels. Moreover, HR reduction in response to vagal stimulation via K_{ACh} channels was augmented by concomitant sympathetic stimulation at 5 Hz vagal stimulation. These findings suggest that the rapidity of response of the vagal HR control via K_{ACh} channels is invariant with respect to background sympathetic tone, and that the magnitude of vagal HR control via K_{ACh} channels is affected by background sympathetic tone in vivo.

This study was supported by Health and Labour Sciences Research Grants H15-Physi-001, H18-Nano-Ippan-003, and H18-Iryo-Ippan-023 from the Ministry of Health, Grants-in-Aid for Scientific Research promoted by the Ministry of Education, Culture, Sports, Science and Technology in Japan 18591992, 19700559, and by the Ground-based Research Announcement for Space Utilization project promoted by the Japan Space Forum. This study was also supported by an Industrial Technology Research Grant Program in 06B44524a from the New Energy and Industrial Technology Development Organization of Japan.

REFERENCES

1. Luetje CW, Tietje KM, Christian JL, Nathanson NM. Differential tissue expression and developmental regulation of guanine nucleotide binding regulatory proteins and their messenger RNAs in rat heart. J Biol Chem. 1988;263:13357-65.
2. Sunahara RK, Dessauer CW, Gilman AG. Complexity and diversity of mammalian adenylyl cyclases. Annu Rev Pharmacol Toxicol. 1996;36:461-80.
3. Huang CL, Slesinger PA, Casey PJ, Jan YN, Jan LY. Evidence that direct binding of G beta gamma to the GIRK1 G protein-gated inwardly rectifying K+ channel is important for channel activation. Neuron. 1995;15:1133-43.
4. Sakmann B, Noma A, Trautwein W. Acetylcholine activation of single muscarinic K+ channels in isolated pacemaker cells of the mammalian heart. Nature. 1983;303:250-3.
5. Yamada M, Inanobe A, Kurachi Y. G protein regulation of potassium ion channels. Pharmacol Rev. 1998;50:723-60.
6. Mizuno M, Kamiya A, Kawada T, Miyamoto T, Shimizu S, Sugimachi M. Muscarinic potassium channels augment dynamic and static heart rate responses to vagal stimulation. Am J Physiol Heart Circ Physiol. 2007;293:H1564-70.
7. Negrão CE, Rondon MU, Tinucci T, Alves MJ, Roveda F, Braga AM, Reis SF, Nastari L, Barretto AC, Krieger EM, Middlekauff HR. Abnormal neurovascular control during exercise is linked to heart failure severity. Am J Physiol Heart Circ Physiol. 2001;280:H1286-92.
8. Mancia G, Grassi G, Giannattasio C, Seravalle G. Sympathetic activation in the pathogenesis of hypertension and progression of organ damage. Hypertension. 1999;34:724-8.
9. Seals DR, Bell C. Chronic sympathetic activation: consequence and cause of age-associated obesity? Diabetes. 2004;53:276-84.
10. Hartzell HC, Méry PF, Fischmeister R, Szabo G. Sympathetic regulation of cardiac calcium current is due exclusively to cAMP-dependent phosphorylation. Nature. 1991;351:573-6.
11. Irisawa H, Brown HF, Giles W. Cardiac pacemaking in the sinoatrial node. Physiol Rev. 1993;73:197-227.
12. Breitwieser GE, Szabo G. Uncoupling of cardiac muscarinic and beta-adrenergic receptors from ion channels by a guanine nucleotide analogue. Nature. 1985;317:538-40.
13. Levy MN. Sympathetic-parasympathetic interactions in the heart. Circ Res. 1971;29:437-45.
14. Kawada T, Ikeda Y, Sugimachi M, Shishido T, Kawaguchi O, Yamazaki T, Alexander J Jr, Sunagawa K. Bidirectional augmentation of heart rate regulation by autonomic nervous system in rabbits. Am J Physiol. 1996;271:H288-95.
15. Kawada T, Uemura K, Kashihara K, Jin Y, Li M, Zheng C, Sugimachi M, Sunagawa K. Uniformity in dynamic baroreflex regulation of left and right cardiac sympathetic nerve activities. Am J Physiol Regul Integr Comp Physiol. 2003;284:R1506-12.
16. Brigham E. FFT transform applications. In: The Fast Fourier Transform and its applications. Englewood Cliffs, NJ: Prentice Hall; 1988. p. 167-203.
17. Bendat J, Piersol A. Single-input/output relationships. In: Random data: analysis and measurement procedures (3rd edition). New York: Wiley; 2000. p. 189-217.
18. Marmarelis P, Marmarelis V. The white noise method in system identification. In: Analysis of physiological systems. New York: Plenum; 1978. p. 131-221.
19. Lavine N, Ethier N, Oak JN, Pei L, Liu F, Trieu P, Rebois RV, Bouvier M, Hebert TE, Van Tol HH. G protein-coupled receptors form stable complexes with inwardly rectifying potassium channels and adenylyl cyclase. J Biol Chem. 2002;277:46010-9.
20. Nikolov EN, Ivanova-Nikolova TT. Coordination of membrane excitability through a GIRK1 signaling complex in the atria. J Biol Chem. 2004;279:23630-6.
21. Kim D. Beta-adrenergic regulation of the muscarinic-gated K+ channel via cyclic AMP-dependent protein kinase in atrial cells. Circ Res. 1990;67:1292-8.
22. Müllner C, Vorobiov D, Bera AK, Uezono Y, Yakubovich D, Frohnwieser-Steinecker B, Dascal N, Schreibmayer W. Heterologous facilitation of G protein-activated K(+) channels by beta-adrenergic stimulation via cAMP-dependent protein kinase. J Gen Physiol. 2000;115:547-58.

Am J Physiol Heart Circ Physiol 295: H1855–H1866, 2008.
First published August 29, 2008; doi:10.1152/ajpheart.522.2008.

Contrasting effects of presynaptic α_2-adrenergic autoinhibition and pharmacologic augmentation of presynaptic inhibition on sympathetic heart rate control

Tadayoshi Miyamoto,[1,2] Toru Kawada,[2] Yusuke Yanagiya,[2] Tsuyoshi Akiyama,[3] Atsunori Kamiya,[2] Masaki Mizuno,[2] Hiroshi Takaki,[2] Kenji Sunagawa,[4] and Masaru Sugimachi[2]

[1]*Department of Physical Therapy, Faculty of Health Sciences, Morinomiya University of Medical Sciences; and* [2]*Department of Cardiovascular Dynamics, Advanced Medical Engineering Center, and* [3]*Department of Cardiac Physiology, National Cardiovascular Center Research Institute, Osaka; and* [4]*Department of Cardiovascular Medicine, Graduate School of Medical Sciences, Kyusyu University, Fukuoka, Japan*

Submitted 16 May 2008; accepted in final form 19 August 2008

Miyamoto T, Kawada T, Yanagiya Y, Akiyama T, Kamiya A, Mizuno M, Takaki H, Sunagawa K, Sugimachi M. Contrasting effects of presynaptic α_2-adrenergic autoinhibition and pharmacologic augmentation of presynaptic inhibition on sympathetic heart rate control. *Am J Physiol Heart Circ Physiol* 295: H1855–H1866, 2008. First published August 29, 2008; doi:10.1152/ajpheart.522.2008.—Presynaptic α_2-adrenergic receptors are known to exert feedback inhibition on norepinephrine release from the sympathetic nerve terminals. To elucidate the dynamic characteristics of the inhibition, we stimulated the right cardiac sympathetic nerve according to a binary white noise signal while measuring heart rate (HR) in anesthetized rabbits ($n = 6$). We estimated the transfer function from cardiac sympathetic nerve stimulation to HR and the corresponding step response of HR, with and without the blockade of presynaptic inhibition by yohimbine (1 mg/kg followed by 0.1 $mg \cdot kg^{-1} \cdot h^{-1}$ iv). We also examined the effect of the α_2-adrenergic receptor agonist clonidine (0.3 and 1.5 $mg \cdot kg^{-1} \cdot h^{-1}$ iv) in different rabbits ($n = 5$). Yohimbine increased the maximum step response (from 7.2 ± 0.8 to 12.2 ± 1.7 beats/min, means ± SE, $P < 0.05$) without significantly affecting the initial slope (0.93 ± 0.23 vs. 0.94 ± 0.22 $beats \cdot min^{-1} \cdot s^{-1}$). Higher dose but not lower dose clonidine significantly decreased the maximum step response (from 6.3 ± 0.8 to 6.8 ± 1.0 and 2.8 ± 0.5 beats/min, $P < 0.05$) and also reduced the initial slope (from 0.56 ± 0.07 to 0.51 ± 0.04 and 0.22 ± 0.06 $beats \cdot min^{-1} \cdot s^{-1}$, $P < 0.05$). Our findings indicate that presynaptic α_2-adrenergic autoinhibition limits the maximum response without significantly compromising the rapidity of effector response. In contrast, pharmacologic augmentation of the presynaptic inhibition not only attenuates the maximum response but also results in a sluggish effector response.

systems analysis; transfer function; α-adrenergic blockade; rabbits

PRESYNAPTIC α_2-ADRENERGIC receptors play an important role in regulating neurotransmitter release in the central and peripheral nervous systems. The concept that neurotransmitter release is modulated by presynaptic autoreceptors was proposed in the 1970s (19, 20, 25, 31–33, 37, 38). Langer (18) first demonstrated that an α-adrenergic antagonist phentolamine, at a concentration below that required to produce its negative chronotropic effect, increases the magnitude of heart rate (HR) response to sympathetic nerve stimulation. Since then, a number of in vivo and in vitro studies have been conducted to characterize the negative feedback regulation of norepinephrine (NE) release via the presynaptic α_2-adrenergic receptors located on the sympathetic nerve terminals (1, 6, 9, 11, 17, 24, 26, 27a, 29, 30, 34, 35). However, the dynamic nature of the presynaptic α_2-adrenergic inhibition in sympathetic HR control remains to be quantified. Because we focus on the effector response to sympathetic nerve stimulation, the term "presynaptic" may be interpreted as "prejunctional" throughout this paper to describe more specifically the NE kinetics at the neuroeffector junction.

We first schematize our hypothesis on the possible modes of operations of the presynaptic inhibition. With reference to Fig. 1, the solid and dotted lines indicate the HR responses with and without the presynaptic inhibition, respectively. Figure 1*A* represents a "limiter-like" operation of the presynaptic inhibition in which the steady-state response is attenuated, while the initial slope of the response is unchanged. Figure 1*B* represents an "attenuator-like" operation in which the steady-state response is attenuated, while the initial slope of the response is also reduced in proportion to the attenuation of the steady-state response. Since the rapid effector response is one of the important hallmarks of neural regulation compared with humoral regulation, determining which of the two operations likely occurs would contribute to the physiological understanding of the presynaptic inhibition. The words "limiter-like" and "attenuator-like" in this paper are used in the specific senses described above.

To answer which of the two operations likely occurs in the presynaptic inhibition, we examined the HR response to dynamic sympathetic nerve stimulation, with or without blocking the α_2-adrenergic receptors in anesthetized rabbits. Because the HR response is mainly mediated by the postsynaptic β_1-adrenergic receptors, the administration of an α_2-adrenergic receptor antagonist does not eliminate the HR response to sympathetic nerve stimulation. We also examined the effects of pharmacologic augmentation of the α_2-adrenergic receptors on the HR response to dynamic sympathetic nerve stimulation. The results of the present study indicated that the presynaptic α_2-adrenergic autoinhibition is a limiter-like operation. In contrast, the pharmacologic

Address for reprint requests and other correspondence: T. Miyamoto, Dept. of Physical Therapy, Faculty of Health Sciences, Morinomiya Univ. of Medical Sciences, Osaka 559-8611, Japan (e-mail: miyamoto@morinomiya-u.ac.jp).

The costs of publication of this article were defrayed in part by the payment of page charges. The article must therefore be hereby marked "*advertisement*" in accordance with 18 U.S.C. Section 1734 solely to indicate this fact.

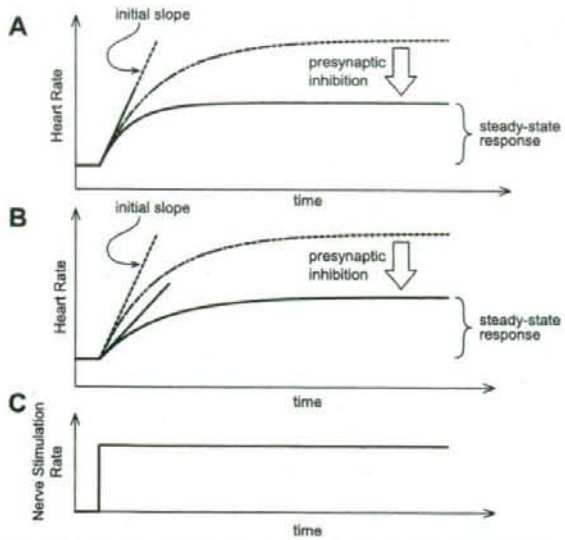

Fig. 1. Schematic representations of the possible operations of the presynaptic inhibition in heart rate (HR) step response to sympathetic nerve stimulation. The solid and dashed lines indicate the HR step response with and without the presynaptic inhibition, respectively. *A*: the presynaptic inhibition attenuates the steady-state response without affecting the initial slope of the response (a "limiter-like" operation). *B*: the presynaptic inhibition attenuates the steady-state response accompanied by a decrease in the initial slope in proportion to the attenuation of the steady-state response (an "attenuator-like" operation). Rapid effector response is maintained in the former but not in the latter. *C*: postulated nerve stimulation rate.

augmentation of presynaptic inhibition is an attenuator-like operation. A possible theoretical explanation for the difference in dynamic characteristics between the presynaptic α_2-adrenergic autoinhibition and the pharmacologic augmentation of the presynaptic inhibition will be proposed.

METHODS

Surgical Preparations

Animal care was in accordance with "Guiding Principles for the Care and Use of Animals in the Field of Physiological Sciences," approved by the Physiological Society of Japan. All protocols were reviewed and approved by the Animal Subject Committee of the National Cardiovascular Center. Japanese white rabbits, weighing 2.5–3.1 kg, were anesthetized by intravenous injection (2 ml/kg) of a mixture of urethane (250 mg/ml) and α-chloralose (40 mg/ml) and mechanically ventilated with oxygen-enriched room air. Tidal volume was set at 35 ml and the rate was adjusted between 35 and 40 cycles/min to be sufficient for suppressing spontaneous respiration. Supplemental doses of these anesthetics were administered by continuous intravenous infusion (1 $ml \cdot kg^{-1} \cdot h^{-1}$) into the marginal ear vein. Arterial pressure (AP) was monitored with a micromanometer catheter (model, Millar Instruments, Houston, TX) inserted into the right femoral artery. A catheter for drug administration was also placed in the right femoral vein. Sinoaortic denervation was performed bilaterally to minimize changes in systemic sympathetic activity via the arterial baroreflexes. The vagi were also sectioned bilaterally at the neck level to remove the vagal control on HR. The right inferior cardiac sympathetic nerve was exposed through a midline thoracotomy and sectioned. A pair of bipolar platinum electrodes was then attached to the cardiac end of the sectioned sympathetic nerve for stimulation (12, 13, 22, 23). The stimulation electrodes and nerve were secured with silicon glue (Kwik-Sil, World Precision Instruments, Sarasota, FL). Instantaneous HR was measured from the AP signal utilizing a cardiotachometer (Tachometer N4778, San-ei, Tokyo, Japan). Body temperature was maintained at 38°C with a heating pad throughout the experiment.

Experimental Procedures

Protocols. To estimate the transfer function from the sympathetic nerve stimulation to HR response, we employed a binary white noise stimulation signal with a switching interval of 5 s. The power spectrum of the sympathetic nerve stimulation rate was fairly constant up to 0.1 Hz and decreased to ~1/10 at 0.15 Hz. The upper frequency limit of the input power that covers the frequency range of physiological interest was determined based on our laboratory's previous studies (12, 23) and also preliminary experimental runs. Different sequences of binary white noise signals were used in different animals. Because HR is linearly related to cardiac output when stroke volume is unchanged, we chose HR as an output signal to understand sympathetic cardiovascular regulation. However, to rule out the possibility that the reciprocal relationship between R-R interval (RRI) and HR confounded the analytical results, we also calculated the transfer function using RRI as an output signal.

In *protocol 1* ($n = 6$), to examine the dynamic nature of the presynaptic α_2-adrenergic autoinhibition, we estimated the transfer function from dynamic sympathetic nerve stimulation to HR response from 20-min data obtained under control and α_2-adrenergic blockade conditions as follows. After recording the control data, an α_2-adrenergic antagonist yohimbine was administered intravenously with an initial bolus injection of 1 mg/kg, followed by continuous infusion at 0.1 $mg \cdot kg^{-1} \cdot h^{-1}$. The yohimbine bolus was equivalent to 10 h of infusion. The duration from the initiation of yohimbine administration until HR and AP reached new steady-state levels was ~15 min (35). We then repeated the 20-min dynamic sympathetic nerve stimulation and recorded the HR response under the α_2-adrenergic blockade condition.

In *protocol 2* ($n = 5$), to examine the effects of pharmacologic augmentation of the presynaptic α_2-adrenergic inhibition on the sympathetic HR control, we estimated the transfer function from dynamic sympathetic nerve stimulation to HR response before and during the administration of an α_2-adrenergic receptor agonist clonidine. Clonidine was administered intravenously at 0.3 and 1.5 $mg \cdot kg^{-1} \cdot h^{-1}$ in an increasing order. After 20-min baseline data collection, we started lower dose clonidine administration and waited for 15 min and then collected data for 20 min. Next, we started higher dose clonidine administration and waited for 15 min and then collected data for 20 min.

The stimulation rate of binary white noise was set at 0–1 Hz for *protocol 1*, and 0–5 Hz for *protocol 2*. Because we expected that blockade of the presynaptic α_2-adrenergic inhibition would augment, whereas activation of the inhibition would attenuate, the HR response, we set a higher stimulation rate for *protocol 2* than for *protocol 1*. The pulse width of sympathetic stimulation was set at 2 ms. The amplitude was set so that 5-Hz tonic sympathetic stimulation produced a HR increase of ~50 beats/min.

As a supplemental protocol, we performed the transfer function analysis using binary white noise signals of 0–1 Hz ($Bin_{0\text{-}1}$), 0–3 Hz ($Bin_{0\text{-}3}$), and 0–5 Hz ($Bin_{0\text{-}5}$) in a random order ($n = 5$). At least a 15-min interval was allowed between the 20-min dynamic sympathetic stimulation trials. The amplitude of sympathetic stimulation was set so that 1-Hz tonic sympathetic stimulation produced a HR increase of ~50 beats/min.

Medetomidine has higher affinity to α_2-adrenergic receptors over α_1-adrenergic receptors compared with clonidine (α_2/α_1 = 1,620:1 for medetomidine, 220:1 for clonidine) (28). However, a preliminary experiment indicated that medetomidine was not as effective as

clonidine to modulate the transfer function from dynamic sympathetic stimulation to HR. Accordingly, we examined the effects of clonidine or medetomidine on myocardial interstitial NE release in response to 5-Hz tonic stimulation (2.5 V, 2-ms pulse width) of the right cardiac sympathetic nerve in vagotomized rabbits. Two microdialysis probes were implanted in the myocardium of the left ventricular free wall. Ringer solution was perfused at 2 μl/min. After a 2-h equilibrium period, we collected 5-min dialysate samples to measure the dialysate NE concentration as an index of myocardial interstitial NE levels (14, 15). High-performance liquid chromatography with electrochemical detection was used to quantify the NE concentration. After the sympathetic stimulation was performed under the control condition, clonidine or medetomidine was intravenously administered (1.5 $mg \cdot kg^{-1} \cdot h^{-1}$). Fifteen minutes later, the sympathetic stimulation was performed under the drug administration condition. Then the drug administration was ceased. Forty-five minutes later, the sympathetic stimulation was performed under the recovery condition. We used different rabbits for clonidine and medatomidine trials. We pooled six dialysate data for statistical analysis.

Data Analysis

Data were digitized at 200 Hz utilizing a 12-bit analog-to-digital converter and stored on the hard disk of a dedicated laboratory computer system. Mean values for HR and AP during dynamic sympathetic nerve stimulation were calculated by averaging the respective data over the stimulation period.

The transfer function from dynamic sympathetic nerve stimulation to HR response was estimated by the following procedures. Twenty minutes of input data (stimulation command) and output data (HR) were resampled at 8 Hz. The resampled data were segmented into eight 50% overlapping bins consisting of 2,048 data points each. The segment length was 256 s. For each segment, the linear trend was subtracted, and a Hanning window was applied. Fast-Fourier transform was then performed to obtain the frequency spectrum of nerve stimulation rate [$N(f)$] and that of HR [$HR(f)$] (5). The power spectral density of the nerve stimulation rate [$S_{N\cdot N}(f)$], that of HR [$S_{HR\cdot HR}(f)$], as well as the cross-spectral density between these two signals [$S_{N\cdot HR}(f)$], were averaged over the eight segments. Finally, the transfer function [$H(f)$] from sympathetic nerve stimulation rate to HR response was calculated using the following equation (2, 21).

$$H(f) = \frac{S_{N\cdot HR}(f)}{S_{N\cdot N}(f)} \quad (1)$$

Transfer function parameters were determined by fitting a second-order, low-pass filter to the estimated transfer function, according to previous studies (12, 13, 23). The second-order, low-pass filter with a pure dead time [$G(f)$] is expressed as

$$G(f) = \frac{K}{1 + 2\zeta \frac{f}{f_N} j + \left(\frac{f}{f_N} j\right)^2} \exp(-2\pi f j L) \quad (2)$$

where K is a steady-state gain, f_N is natural frequency (in Hz), ζ is a damping ratio, L is pure dead time (in s), and j indicates an imaginary unit. A schematic explanation for these transfer function parameters is provided in the APPENDIX. To estimate the parameters, an iterative nonlinear least squares fitting was performed to minimize the following error function.

$$\text{error} = \frac{\sum_{k=1}^{n} |G(f) - H(f)|^2}{\sum_{i=1}^{n} |H(f)|^2}, \quad f = f_0 \times k \quad (3)$$

where f_0 is the fundamental frequency of the discrete Fourier transform, $f_0 = 1/256 = 0.004$ Hz, and k is a frequency index. The n represents the upper limit of the frequency index determined from the range of sufficient input power in the sympathetic nerve stimulation; $n = 40$, $f_0 \times n = 0.156$ Hz.

To quantify the linear dependence of the HR response on the sympathetic nerve stimulation, the magnitude-squared coherence function [$\gamma^2(f)$] was calculated by the following equation (2, 21).

$$\gamma^2(f) = \frac{|S_{N\cdot HR}(f)|^2}{S_{N\cdot N}(f) \cdot S_{HR\cdot HR}(f)} \quad (4)$$

The coherence value ranges from zero to unity. The unity coherence value indicates a perfect linear dependence between the input and output signals, whereas zero coherence indicates a total independence between the two signals.

To facilitate the intuitive understanding of the HR response to dynamic sympathetic nerve stimulation, we calculated the step response from the estimated transfer function. The step response was obtained from the time integral of the system impulse response derived from the inverse Fourier transform of the transfer function. The steady-state response was calculated by averaging the step response during the last 10 s of the 128-s response. To characterize the rising speed of the step response, the initial slope for the response was calculated as follows. An analysis of linear regression with a slope and an intercept was performed on the initial data points of the step response while varying the number of data points from 2 to 1,024. The maximum slope obtained was used as the initial slope of the response. The linear regression was performed, including the portion of the dead time. Although including the dead time reduced the maximum slope, the effect was small because the number of data points that yielded the maximum slope (~90 points) was much larger than that for the dead time (<10 points). The step response of RRI was also calculated from the corresponding transfer function from sympathetic nerve stimulation to RRI.

Statistics

All data are presented as means ± SE. In *protocol 1*, mean HR, AP, and transfer function parameters were compared before and during yohimbine administration by paired *t*-tests. In *protocol 2*, the data were compared among control, lower dose, and higher dose clonidine conditions using a repeated-measures ANOVA followed by Dunnett's test against the single control (8). In the supplemental protocol of the transfer function analysis, the data were compared among $Bin_{0\text{-}1}$, $Bin_{0\text{-}3}$, and $Bin_{0\text{-}5}$ stimulus conditions using a repeated-measures ANOVA followed by Tukey test for all pairwise comparisons. In the supplemental protocol of the NE measurement, baseline NE levels were compared before and during drug administration using a paired *t*-test. The NE levels during sympathetic stimulation were compared among control, drug administration, and recovery conditions using a repeated-measures ANOVA followed by Dunnett's test against the control condition. In all of the statistical procedures, the difference was considered significant at $P < 0.05$.

RESULTS

Figure 2*A* represents a typical recording obtained from *protocol 1*. We stimulated the cardiac sympathetic nerve according to a binary white noise signal and recorded HR response under control condition and during yohimbine administration. The presynaptic α_2-adrenergic negative feedback mechanism functioned under the control condition but not during yohimbine administration. HR changed dynamically in response to the random sympathetic nerve stimulation under both conditions. Yohimbine increased the magnitude of HR variation. The augmentation of sympathetic effect was also observed in the RRI response. Although yohimbine decreased the mean level of HR in this animal, changes in mean HR

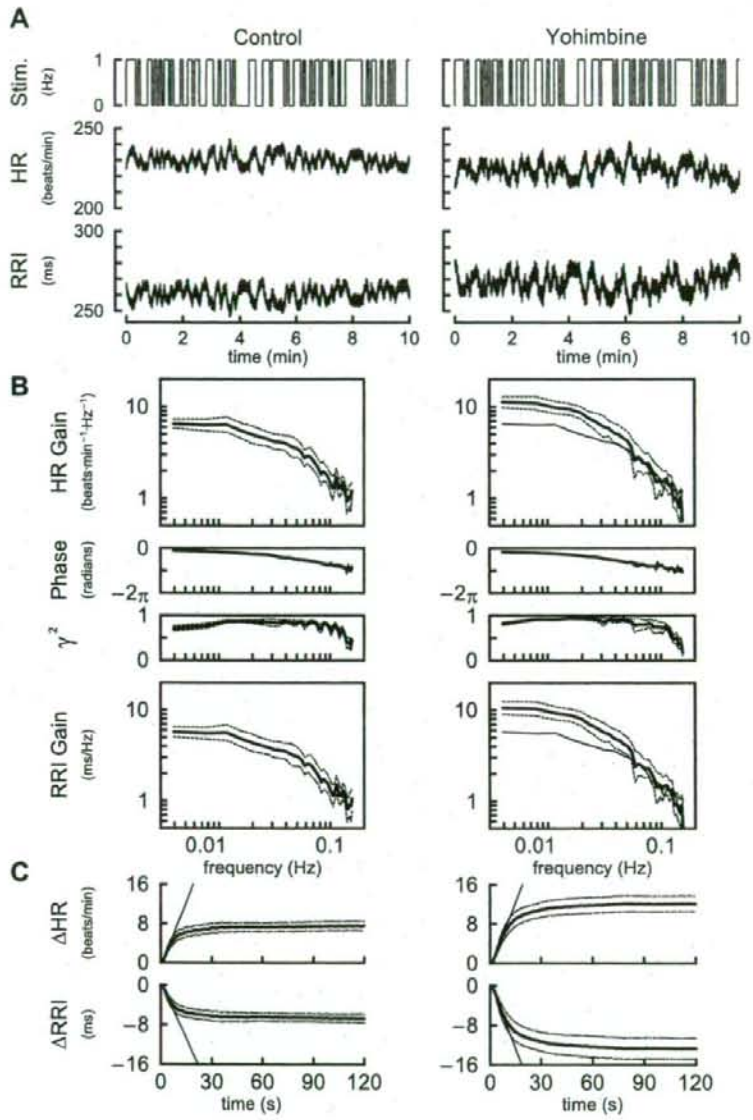

Fig. 2. *A:* representative recordings of cardiac sympathetic nerve stimulation rate (Stim; *top*), HR response (*middle*), and R-R interval (RRI) response (*bottom*) under conditions of control (*left*) and yohimbine administration (*right*) obtained in *protocol 1*. Yohimbine blocks the presynaptic α_2-adrenergic autoinhibition. The amplitude of HR variation and that of RRI variation become greater in the presence of yohimbine. *B:* transfer functions averaged over all animals in *protocol 1*. HR gain plots (*top*), phase plots (*second*), coherence functions (γ_2, *third*), and RRI gain plots (*bottom*). Yohimbine increases the dynamic gain in the frequency range between 0.004 and 0.04 Hz but not in the higher frequency range. The fine solid curve in the gain (*right*) duplicates the mean gain plot (*left*). *C:* step responses of HR (*top*) and RRI (*bottom*) calculated from the corresponding transfer functions. Yohimbine augments the steady-state response without affecting the initial slope of the response (fine oblique line). Bold, solid lines represent the mean, whereas dotted lines indicate means ± SE.

varied among the animals and were not significantly different between the control and yohimbine conditions.

Table 1 summarizes the mean HR and AP averaged from the six animals. The α_2-adrenergic blockade by yohimbine did not significantly affect the HR or AP before sympathetic nerve stimulation. Yohimbine also did not affect HR or AP significantly during the stimulation period.

Figure 2*B* illustrates the transfer functions averaged from the six animals in *protocol 1*. In the HR gain plots, the gain value was relatively constant <0.01 Hz and decreased >0.01 Hz, indicating low-pass filter characteristics of the HR response to sympathetic nerve stimulation. Yohimbine increased the HR gain from 7.1 ± 0.7 to 12.0 ± 1.7 beats·min^{-1}·Hz^{-1} at the lowest frequency of 0.004 Hz ($P < 0.05$). In contrast, yohimbine did not affect the HR gain value at 0.1 Hz (1.8 ± 0.4 vs. 1.7 ± 0.6 beats·min^{-1}·Hz^{-1}). The solid fine curve in the *right* panel duplicates the mean gain plot in the *left* panel as a reference. In the phase plots, the phase value approached zero radians at the lowest frequency and lagged with increasing frequency under both conditions. In the coherence function plots, the coherence was >0.8 in the frequency range from 0.01 to 0.08 Hz, suggesting that the HR response to sympathetic nerve stimulation in this frequency range can be explained reasonably well by linear dynamics for both conditions. Changes in the RRI gain plots were similar to those in the HR gain plots. Yohimbine increased the RRI gain from

Table 1. *Mean heart rate and arterial pressure before and during random stimulation of the cardiac sympathetic nerve*

	Control	Yohimbine
Heart rate, beats/min		
Before	259±15	244±13
During	264±15	254±17
Mean arterial pressure, mmHg		
Before	90±8	87±6
During	91±9	88±8

Values are means ± SE. Data were obtained after vagal and cardiac sympathetic nerves were cut. No statistically significant difference was detected between control vs. yohimbine values by paired *t*-tests.

6.0 ± 0.7 to 11.3 ± 1.9 ms/Hz at the lowest frequency of 0.004 ($P < 0.05$) but not at 0.1 Hz (1.8 ± 0.4 vs. 1.9 ± 0.8 ms/Hz). Given the inverse relationship between RRI and HR, the RRI phase plots (not shown) quite resembled to the corresponding HR phase plots except for the rotation by π radians.

Figure 2*C* represents the step responses of HR to sympathetic nerve stimulation calculated from the transfer functions shown in Fig. 2*B*. Yohimbine increased the steady-state response significantly (Table 2). The initial slope of the response, depicted by an oblique straight line, was not affected by yohimbine (Table 2). In the RRI step response, yohimbine augmented the steady-state response from −6.7 ± 0.9 to −12.6 ± 2.1 ms ($P < 0.05$) without affecting the initial slope (−0.71 ± 0.18 vs. −0.90 ± 0.23 ms/s).

Parameters of the transfer functions and step responses estimated in *protocol 1* are summarized in Table 2. The steady-state gain was significantly greater and the natural frequency was significantly lower in yohimbine condition compared with control. The damping coefficient and pure dead time did not differ significantly between the control and yohimbine conditions. Whereas the steady-state response was significantly increased by yohimbine, the initial slope of the step response was not significantly changed.

Figure 3*A* represents a typical recording of the sympathetic nerve stimulation and HR response obtained from *protocol 2*. The effects of α_2-adrenergic stimulation by clonidine were tested at two doses. Lower dose clonidine did not affect the magnitude of HR variation. Although lower dose clonidine decreased the mean HR in this animal, changes in the mean HR were not significantly different among the animals (Table 3). Higher dose clonidine significantly attenuated the magnitude of HR variation and also decreased mean HR. The attenuation of sympathetic effect was also observed in the RRI response during the high-dose clonidine administration.

Table 3 summarizes the mean HR and AP obtained from *protocol 2*. Higher dose, but not lower dose, clonidine significantly decreased the mean HR, both before and during cardiac sympathetic nerve stimulation. Clonidine did not affect mean AP significantly, before or during cardiac sympathetic nerve stimulation.

Figure 3*B* illustrates the transfer functions averaged from the five animals in *protocol 2*. Lower dose clonidine did not affect the transfer function significantly. In the HR gain plots, higher dose clonidine decreased the gain from 6.6 ± 0.9 to 2.7 ± 0.5 beats·min^{-1}·Hz^{-1} at the lowest frequency of 0.004 Hz ($P < 0.05$) and from 1.1 ± 0.2 to 0.5 ± 0.2 beats·min^{-1}·Hz^{-1} at the frequency of 0.1 Hz ($P < 0.05$). Higher dose clonidine did not affect the phase plot significantly. In the coherence function plots, the coherence was >0.8 in control and lower dose clonidine conditions and >0.7 in higher dose clonidine condition for the frequency range from 0.01 to 0.08 Hz, suggesting that the HR response to sympathetic nerve stimulation can be explained reasonably well by linear dynamics in all three conditions. Although relative change became smaller compared to the HR gain plots, the attenuation of transfer gain was also observed in the RRI gain plots. Higher-dose clonidine decreased the gain from 4.5 ± 0.7 to 2.8 ± 0.5 ms/Hz at the lowest frequency of 0.004 Hz ($P < 0.05$) and from 0.88 ± 0.19 to 0.04 ± 0.09 ms/Hz at the frequency of 0.1 Hz ($P < 0.05$).

Figure 3*C* represents the step responses of HR to sympathetic nerve stimulation calculated from the transfer functions shown in Fig. 3*B*. Lower dose clonidine did not affect either the steady-state response or the initial slope of the step response. In contrast, higher dose clonidine attenuated the steady-state response and also reduced the initial slope of the response. In the RRI step response, higher-dose clonidine attenuated the steady-state response from −4.9 ± 0.7 to −3.0 ± 0.6 ms ($P < 0.05$) with a significant reduction in the initial slope from −0.40 ± 0.07 to −0.23 ± 0.05 ms/s ($P < 0.05$).

Parameters of the transfer functions and step responses estimated in *protocol 2* are summarized in Table 4. The steady-state gain of the transfer function and the steady-state response of the corresponding step response were decreased by higher dose but not by lower dose clonidine. The initial slope of the step response was decreased by higher dose clonidine. The ratio of the steady-state response to the initial slope was unchanged. The natural frequency and the damping ratio of the transfer function were not affected by clonidine. The pure dead time of the transfer function was increased by lower dose, but not by higher dose, clonidine.

Figure 4*A* represents a typical recording of the sympathetic nerve stimulation and HR response obtained from the supplemental protocol. The binary white noise signals of the same sequence but different stimulus rate were applied. Increasing the stimulus rate augmented the magnitude of HR variation and increased mean HR. The increase was not proportional to the increase in the stimulus rate, however, because of the saturation of HR response to sympathetic nerve stimulation. The increase of RRI variation was not proportional to the increase in the stimulus rate either, suggesting that the saturation effect observed in the HR response was not an artifact of reciprocal relationship between RRI and HR.

Table 2. *Parameters of the transfer functions and step responses*

	Control	Yohimbine
K, beats·min^{-1}·Hz^{-1}	7.3±1.1	12.0±2.1*
f_N, Hz	0.081±0.012	0.055±0.008*
ζ	1.64±0.47	1.55±0.21
L, s	0.82±0.22	1.03±0.19
Fitting error, %	5.6±1.5	3.6±1.1
S, beats/min	7.2±0.8	12.2±1.7*
α, beats·min^{-1}·s^{-1}	0.93±0.23	0.94±0.22
S/α, s	9.1±1.4	14.4±1.9*

Values are means ± SE. K, steady-state gain; f_N, natural frequency; ζ, damping coefficient; L, pure dead time; S, steady-state response; α, initial slope; S/α, ratio of S to α. *$P < 0.05$ vs. control values.

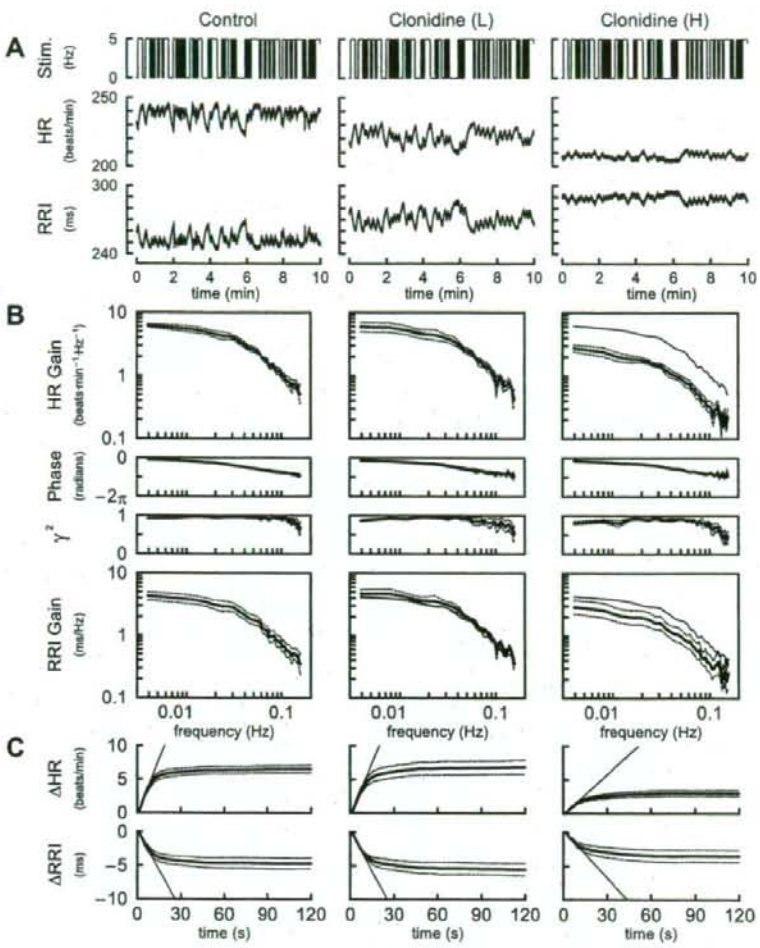

Fig. 3. *A:* representative recordings of cardiac sympathetic nerve stimulation rate (*top*), HR response (*middle*), and RRI response (*bottom*) under conditions of control (*left*), lower-dose clonidine (0.3 $mg \cdot kg^{-1} \cdot h^{-1}$; *middle*), and higher-dose clonidine (1.5 $mg \cdot kg^{-1} \cdot h^{-1}$; *right*) obtained in *protocol 2*. Clonidine activates the presynaptic α_2-adrenergic inhibition independent of the amount of norepinephrine released at the sympathetic nerve terminals. The amplitude of HR variation becomes smaller, and the mean level of HR becomes lower in the presence of higher-dose clonidine. The amplitude of RRI response also became smaller under higher-dose clonidine condition. *B:* transfer functions averaged over all animals in *protocol 2*. HR gain plots (*top*), phase plots (*second*), coherence functions (γ_2, *third*), and RRI gain plots (*bottom*). Lower-dose clonidine does not affect the transfer function significantly. Higher-dose clonidine decreases the dynamic gain in the whole frequency range (0.004 to 0.2 Hz). The fine solid curves in the gain plots (*middle* and *right*) duplicate the mean gain plot (*left*). *C:* step responses of HR (*top*) and RRI (*bottom*) calculated from the corresponding transfer functions. Lower-dose clonidine does not affect the step response significantly. Higher-dose clonidine attenuates the steady-state response accompanied by a decrease in the initial slope of the response (fine oblique line). Bold, solid lines represent the mean, whereas dotted lines indicate means ± SE.

Table 5 summarizes the mean HR and AP obtained from the supplemental protocol. There were no significant differences in mean HR and AP before cardiac sympathetic nerve stimulation. Mean HR was higher in $Bin_{0\text{-}3}$ and $Bin_{0\text{-}5}$ than in $Bin_{0\text{-}1}$ condition. Mean AP did not differ among the three conditions.

Figure 4*B* illustrates the transfer function averaged from the five animals in the supplemental protocol. The contour of HR gain plots showed an approximately downward shift with increase in the stimulus rate of the binary white noise signal, indicating that the augmentation of the HR variation seen in Fig. 4*A* was not proportional to the increase in the stimulus rate. No significant differences were noted in the phase plot. The coherence values were slightly decreased in all frequencies with increase in the stimulus rate of the binary white noise signal, suggesting that the HR response became saturated and the linearity between the stimulation and the HR response was

Table 3. *Mean heart rate and arterial pressure before and during random stimulation of the cardiac sympathetic nerve*

	Control	Clonidine (L)	Clonidine (H)
Heart rate, beats/min			
Before	277±16	250±15	232±20*
During	299±14	271±14	246±27*
Mean arterial pressure, mmHg			
Before	95±6	77±8	113±9
During	96±6	79±9	115±13

Values are means ± SE. Data were obtained after vagal and cardiac sympathetic nerves were cut. *$P < 0.05$ vs. control values by Dunnett's test.

Table 4. *Transfer function parameters and step responses*

	Control	Clonidine (L)	Clonidine (H)
K, $beats \cdot min^{-1} \cdot Hz^{-1}$	6.4±0.8	6.8±1.1	2.7±0.5*
f_N, Hz	0.066±0.017	0.070±0.016	0.059±0.013
ζ	1.56±0.37	1.72±0.23	1.55±0.20
L, s	0.56±0.17	1.24±0.20*	1.03±0.18
Fitting error, %	2.9±1.2	4.2±1.5	5.5±2.3
S, beats/min	6.3±0.8	6.8±1.0	2.8±0.5*
α, $beats \cdot min^{-1} \cdot s^{-1}$	0.56±0.07	0.51±0.04	0.22±0.06*
S/α, s	11.2±0.7	13.1±1.3	13.8±1.2

Values are means ± SE. *$P < 0.05$ vs. control values.

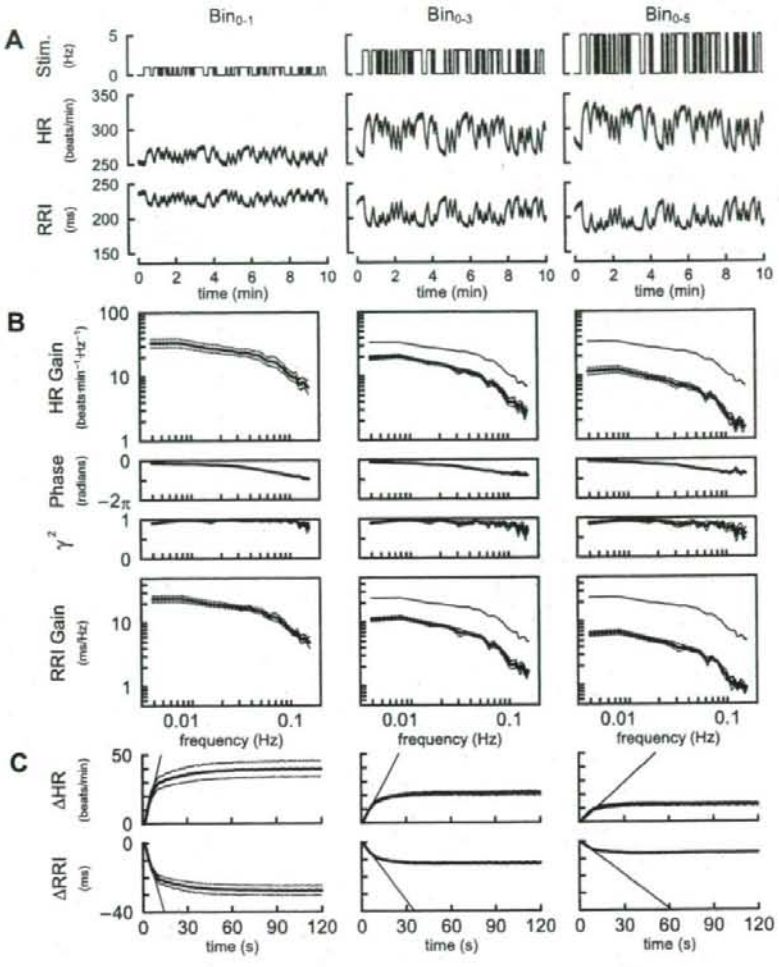

Fig. 4. *A*: representative recordings of cardiac sympathetic nerve stimulation rate (*top*), HR response (*middle*), and RRI response (*bottom*) obtained by differing the stimulus rate of the binary white noise signal. Bin_{0-1}, binary white noise between 0 and 1 Hz; Bin_{0-3}, binary white noise between 0 and 3 Hz; Bin_{0-5}, binary white noise between 0 and 5 Hz. Increasing the stimulus rate of the binary white noise signal augments the magnitude of HR response and increased mean HR. The RRI response was also increased with increasing the stimulus rate. *B:* transfer functions averaged over all animals in the supplemental protocol. HR gain plots (*top*), phase plots (*second*), coherence functions (γ_2, *third*), and RRI gain plots (*bottom*). Increasing the stimulus rate of the binary white noise signal decreases the dynamic gain in the whole frequency range (0.004 to 0.2 Hz). The fine solid curves in the gain plots (*middle* and *right*) duplicate the mean gain plot (*left*). *C:* step responses of HR (*top*) and RRI (*bottom*) calculated from the transfer functions. Increasing the stimulus rate of the binary white noise signal attenuates the steady-state response accompanied by a decrease in the initial slope of the response (fine oblique line). Bold, solid lines represent the mean, whereas dotted lines indicate means ± SE.

slightly reduced in Bin_{0-3} and Bin_{0-5} compared with that in Bin_{0-1} condition. The contour of RRI gain plots also showed approximately downward shift with increasing the stimulus rate of the binary white noise signal.

Figure 4*C* represents the step response of HR to sympathetic nerve stimulation calculated from the transfer functions shown in Fig. 4*B*. The increase in the stimulus rate of the binary white noise signal attenuated the steady-state response and also reduced the initial slope of the response. In the RRI step

Table 5. *Mean heart rate and arterial pressure before and during random stimulation of the cardiac sympathetic nerve*

	Bin_{0-1}	Bin_{0-3}	Bin_{0-5}
Heart rate, beats/min			
Before	268±6	269±7	266±5
During	292±8	330±9*	341±11*
Mean arterial pressure, mmHg			
Before	84±7	82±5	88±12
During	94±7	94±7	95±9

Values are means ± SE. Data were obtained after vagal and cardiac sympathetic nerves were cut. Bin_{0-1}, Bin_{0-3}, and Bin_{0-5}: binary white noise signals of 0–1, 0–3, and 0–5 Hz, respectively. *$P < 0.01$ vs. Bin_{0-1} values by Tukey test. There were no significant differences in parameters between Bin_{0-3} and Bin_{0-5}.

Table 6. *Transfer function parameters and step responses*

	Bin_{0-1}	Bin_{0-3}	Bin_{0-5}
K, beats·min^{-1}·Hz^{-1}	36.2±4.9	20.0±1.1†	11.8±1.1†
f_N, Hz	0.098±0.009	0.079±0.006*	0.078±0.006*
Z	1.56±0.04	1.68±0.04*	1.68±0.05*
L, s	0.95±0.01	0.97±0.01	0.97±0.01
Fitting error, %	4.8±1.1	3.2±0.8	3.5±0.5
S, beats/min	40.9±5.1	22.1±1.6†	12.8±1.4†
α, beats·min^{-1}·s^{-1}	4.23±0.61	2.00±0.21†	1.20±0.17†
S/α, s	9.9±0.5	11.3±0.8	10.8±0.8

Values are means ± SE. †$P < 0.01$ and *$P < 0.05$ vs. Bin_{0-1} values by Tukey test. There were no significant differences in parameters between Bin_{0-3} and Bin_{0-5}.

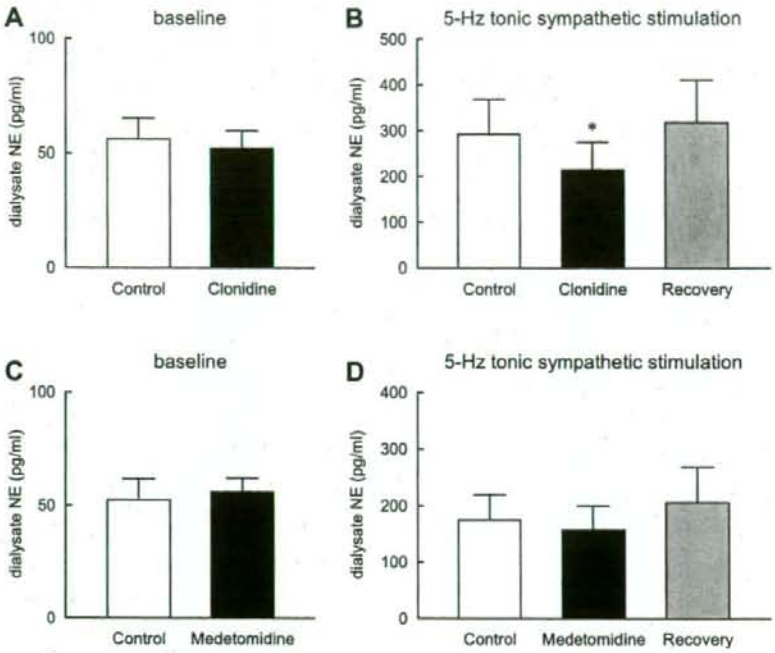

Fig. 5. Effects of clonidine (1.5 mg·kg^{-1}·h^{-1} iv) or medetomidine (1.5 mg·kg^{-1}·h^{-1} iv) on the myocardial interstitial norepinephrine (NE) release in response to 5-Hz tonic cardiac sympathetic nerve stimulation. Data were obtained after sectioning vagal and cardiac sympathetic nerves. Clonidine administration does not affect baseline levels of NE (*A*), but significantly attenuates the stimulation-induced NE release (*B*). *C*: medetomidine administration does not affect baseline levels of NE. *D*: it does not attenuate the stimulation-induced NE release significantly. Values are means ± SE. *$P < 0.05$ from control.

response, the steady-state response was attenuated from -27.6 ± 2.8 to -12.2 ± 0.7 ($P < 0.01$) and -6.7 ± 0.4 ($P < 0.01$) ms during Bin_{0-3} and Bin_{0-5}, respectively. The initial slope was attenuated from -3.0 ± 0.3 to -1.1 ± 0.1 ($P < 0.01$) and -0.65 ± 0.06 ($P < 0.01$) ms/s during Bin_{0-3} and Bin_{0-5}, respectively.

Parameters of the transfer functions and step responses estimated in the supplemental protocol are summarized in Table 6. The steady-state gain of the transfer function and the steady-state response of the corresponding step response decreased with increase in the stimulus rate of the binary white noise sequence. Although the initial slope of the step response significantly decreased with increase in the stimulus rate of the binary white noise signal, the ratio of the steady-state response to the initial slope was unchanged. The natural frequency was lower and the damping coefficient was greater in Bin_{0-3} and Bin_{0-5} than Bin_{0-1} condition. The pure dead time of the transfer function did not differ among the three conditions.

Figure 5 summarizes the results of the supplemental protocol of NE measurement. Baseline levels of myocardial interstitial NE did not differ before and during clonidine administration (Fig. 5*A*). Clonidine administration attenuated the sympathetic stimulation-induced NE release to 75.8 ± 5.4% of the control ($P < 0.05$) (Fig. 5*B*). Baseline NE levels did not differ before and during medetomidine administration (Fig. 5*C*). Medetomidine did not attenuate the sympathetic stimulation-induced NE release significantly (92.0 ± 6.7% of the control, not significant) (Fig. 5*D*).

Simulation Study

To explore possible mechanisms for the observed differences between the presynaptic α_2-adrenergic autoinhibition and the pharmacologic augmentation of the presynaptic inhibition via the α_2-adrenergic receptors, we performed a simulation on the negative feedback regulation of the HR response to the sympathetic nerve stimulation. With reference to Fig. 6*A*, H_{FW} and H_{FB} represent the transfer functions of the forward path and the feedback path, respectively. A step input signal represents the sympathetic nerve stimulation. Both signals from presynaptic α_2-adrenergic autoinhibition and pharmacologic augmentation of the presynaptic inhibition attenuate the input signal via the same α_2-adrenergic receptors. Because the amount of neurotransmitter release cannot become negative, a threshold operator (Th) is added. The threshold operator is described mathematically as follows.

$$\mathrm{Th}(x) = x \text{ when } x > 0, \text{ otherwise } \mathrm{Th}(x) = 0$$

The output from the threshold operator or the amount of neurotransmitter is then fed into H_{FW} to yield the output or change in HR and is also fed into H_{FB} to yield the feedback signal of presynaptic α_2-adrenergic autoinhibition. Since we administered clonidine ~15 min before sympathetic nerve stimulation, the effect of clonidine should have reached the steady state at the time of sympathetic nerve stimulation. Accordingly, we treated the pharmacologic augmentation of the presynaptic inhibition as a constant input. The magnitude of pharmacologic augmentation of the presynaptic inhibition was set arbitrarily to 0.5 to mimic the results of higher dose clonidine in *protocol 2*. The simulation was conducted using Matlab Simulink (The Mathworks, Natick, MA).

Yohimbine administration corresponds to severing the feedback path, i.e., setting $H_{FB} = 0$ in the simulation. Under this condition, the transfer function from the input to output becomes H_{FW}. Therefore, we modeled H_{FW} using the second-order, low-pass filter with pure dead time (*Eq. 3*) with the

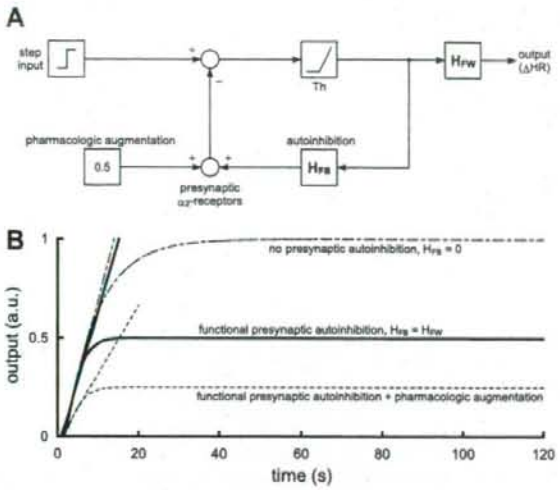

Fig. 6. Possible theoretical explanation for the differential effects of presynaptic α_2-adrenergic autoinhibition and pharmacologic augmentation of presynaptic α_2-adrenergic inhibition on the HR response to sympathetic nerve stimulation. *A:* a simulation model for the HR step response to a step input in the sympathetic nerve activity. H_{FW}, transfer function of the forward path; H_{FB}, transfer function of the feedback path; Th, a threshold operator (see main text for details). *B:* simulation results under conditions of no presynaptic inhibition (dash-dot line; H_{FB} = 0 and pharmacologic augmentation of presynaptic inhibition = 0, corresponding to the yohimbine administration condition), functional presynaptic α_2-adrenergic autoinhibition (solid line; H_{FB} = H_{FW} and pharmacologic augmentation of presynaptic inhibition = 0, corresponding to the control condition), and functional presynaptic α_2-adrenergic autoinhibition plus pharmacologic augmentation of the presynaptic inhibition (dotted line; H_{FB} = H_{FW} and pharmacologic augmentation of presynaptic inhibition = 0.5, corresponding to the higher-dose clonidine condition). The presynaptic α_2-adrenergic autoinhibition does not attenuate the initial slope of the step response. In contrast, the pharmacologic augmentation of the presynaptic inhibition attenuates the initial slope of the step response.

settings of f_N = 0.055, ζ = 1.55, and L = 0.94 (Table 2, yohinbine). The gain was set at unity for simplicity. With this setting, we calculated the output response to the unit step input without the presynaptic inhibition (Fig. 6*B*, dash-dot line, corresponding to the yohimbine condition). The initial slope of the response, calculated from the linear regression analysis described in the method section, was 0.0763 arbitrary units (AU)/s. Next, we set H_{FB} = H_{FW} and performed a simulation of the condition with the presynaptic α_2-adrenergic autoinhibition (Fig. 6*B*, solid line, corresponding to the control condition). The presynaptic α_2-adrenergic autoinhibition attenuates the steady-state response without significantly affecting the initial slope of the response (0.0695 AU/s). Finally, we set the pharmacologic augmentation of the presynaptic inhibition to 0.5 on top of the functioning H_{FB}. The simulation result (Fig. 6*B*, dotted line, corresponding to the higher dose clonidine condition) demonstrates that pharmacologic augmentation of the presynaptic inhibition attenuates the steady-state response accompanied by a reduction in the initial slope of the response (0.0346 AU/s).

DISCUSSION

We compared the blockade and activation of the presynaptic α_2-adrenergic receptors and found a difference between the presynaptic α_2-adrenergic autoinhibition and the pharmacologic augmentation of the presynaptic inhibition in terms of HR response to sympathetic nerve stimulation. The presynaptic α_2-adrenergic autoinhibition showed a limiter-like operation that restricts the steady-state response without affecting the initial slope of the response. In contrast, the pharmacologic augmentation of presynaptic inhibition showed an attenuator-like operation that reduces both the steady-state response and the initial slope of the response.

Comparison of Blocking and Activating the Presynaptic α_2-Adrenergic Receptors

Although the presynaptic α_2-adrenergic negative feedback has been known to attenuate the NE release and HR response to sympathetic nerve stimulation (9, 21, 26, 27, 29, 30, 31), the dynamic nature of the negative feedback remained to be elucidated. As shown in Fig. 2*C*, the blockade of α_2-adrenergic receptors by yohimbine increased the steady-state response without significantly affecting the initial slope of the HR step response (Table 2). That is to say, the presynaptic α_2-adrenergic autoinhibition of the presynaptic inhibition attenuates the steady-state response without sacrificing the rising speed of HR response to sympathetic nerve stimulation under control condition. These characteristics of the presynaptic α_2-adrenergic autoinhibition conform to the limiter-like operation shown in Fig. 1*A*. In contrast, pharmacologic augmentation of the presynaptic inhibition by higher dose clonidine reduced the steady-state response accompanied by a decrease in the initial slope of the HR step response (Fig. 3*C*). The ratio of the steady-state response to the initial slope was not changed significantly by higher dose clonidine (Table 4), suggesting that attenuation of the initial slope was proportional to that of the steady-state response. These characteristics of the pharmacologic augmentation of the presynaptic inhibition conform to the attenuator-like operation shown in Fig. 1*B*. Rapid effector response is one of the most important hallmarks of neural regulation compared with humoral regulation. The findings of the present study suggest that presynaptic α_2-adrenergic autoinhibition, but not pharmacologic augmentation of the presynaptic α_2-adrenergic inhibition, prevents excess NE outflow at the sympathetic nerve terminals without compromising the rapidity of effector response. The simulation results suggest that the initial slope of the response decreases when presynaptic inhibition occurs, independent of the negative feedback mechanism (Fig. 6*B*). On the other hand, the initial slope of the response does not decrease significantly when the presynaptic inhibition occurs through the negative feedback mechanism.

α_2-Adrenergic receptors are classified as α_{2A}-, α_{2B}-, and α_{2C}-subtypes based on gene encodings (26). Furthermore, the different ligand binding characteristics of the α_{2A}-subtype give rise to the pharmacological subtype of α_{2A} in humans, rabbits, and pigs and that of α_{2D} in rats, mice, and guinea pigs (26). The α_{2A} and α_{2D} may be considered as "orthologous" α_2-receptors, with only one being present in any given species (27). In the sympathetic nerve, α_{2A}- and α_{2C}-receptors operate as presynaptic inhibitory autoreceptors, whereas α_{2B}-receptors are located on postsynaptic cells to mediate the effects of catecholamine, such as vasoconstriction (26). In tissue slices from mouse atria, α_{2A}-receptors inhibit NE release from sympathetic nerves primarily at high-stimulation rates (1–2 Hz), whereas

α_{2C}-receptors can operate at very low stimulation rates (0.05–0.1 Hz) (10). Because α_2-receptors in the rabbit heart are characterized as α_{2A}, changes in the transfer function from sympathetic nerve stimulation to HR response observed in the present study are most likely mediated by α_{2A}-receptors.

Clonidine administration (5 μg/kg bolus followed by 30 $\mu g \cdot kg^{-1} \cdot h^{-1}$ iv) attenuated the sympathetic outflow from the central nervous system in rabbits (35). However, lower dose clonidine at 0.3 $mg \cdot kg^{-1} \cdot h^{-1}$ failed to significantly affect the steady-state response or the initial slope of the HR step response in the present study (Fig. 3*B*, Table 4), suggesting a difference in clonidine sensitivity between the central and peripheral sympathetic nervous systems. Another factor that should be taken into account is the operating range of the HR control (i.e., mean HR during dynamic sympathetic stimulation). As an example, tonic vagal stimulation decreased mean HR during dynamic sympathetic stimulation, which increased the dynamic gain of sympathetic HR control via nonlinear sigmoidal input-output nature between autonomic activities and HR (12, 13). Therefore, the decrease in the mean HR during lower dose clonidine, although it was statistically insignificant (Table 3), should have an effect of increasing the dynamic gain of the sympathetic HR control. Such an effect might have counterbalanced the effect of reducing the dynamic gain via presynaptic inhibition during the lower dose clonidine administration. Although higher dose clonidine decreased mean HR before and during sympathetic nerve stimulation, mean AP did not decrease compared with lower dose clonidine (Table 3). The discrepancy between the changes in mean HR and AP may be due to direct vasoconstriction by higher dose clonidine through α-adrenergic stimulation.

Transfer Function Analysis vs. Step Response Analysis

In a previous study, our laboratory performed a transfer function analysis on the sympathetic HR control using a binary white noise signal (12, 23). The transfer function is a frequency-domain representation of the system dynamic characteristics over a wide frequency range and is useful for understanding the behavior of the system in response to a variety of input signals (3, 7, 21). Notwithstanding the theoretical advantages of the transfer function, the frequency-domain representation may be somewhat unfamiliar to most physiologists. Therefore, we calculated the step responses corresponding to the transfer functions. As can be seen in Figs. 2, *B* and *C* and 3, *B* and *C*, changes in transfer function in the lower frequency range reflect the steady-state response in the step response. Changes in transfer function in the higher frequency reflect the initial transient response in the step response. Because the step response and the transfer function are mathematically interchangeable, both the transfer function and the step response provide comparable information on the system dynamic characteristics.

In a previous study, our laboratory has shown that increasing mean stimulus rate of the Gaussian white noise decreased the steady-state gain of the transfer function from sympathetic nerve stimulation to HR without affecting the natural frequency or damping coefficient significantly (23). Increasing the stimulus rate of the binary white noise signal also caused an approximately parallel downward shift in the gain plot (Fig. 4*B*). The transfer function parameters, however, showed a decrease in the natural frequency and an increase in the damping coefficient (Table 6). The higher natural frequency in $Bin_{0\text{-}1}$ than in $Bin_{0\text{-}5}$ condition may account for the higher natural frequency in *protocol 1* ($Bin_{0\text{-}1}$ was used for sympathetic stimulation) than in *protocol 2* ($Bin_{0\text{-}5}$ was used for sympathetic stimulation) observed under control conditions. Notwithstanding the differences in the natural frequency and the damping coefficient, the ratio of the step response to the initial slope was not changed significantly by the difference in the stimulus rate of the binary white noise signal. Therefore, yohimbine-induced changes in the ratio of the step response to the initial slope observed in *protocol 1* (Table 1) cannot be explained by changes in the magnitude of sympathetic effect on HR.

Limitations

The present study has several limitations. First, we performed the experiment under anesthetic conditions. However, because we compared the effects of yohimbine and clonidine on the sympathetic HR control under the same anesthetic

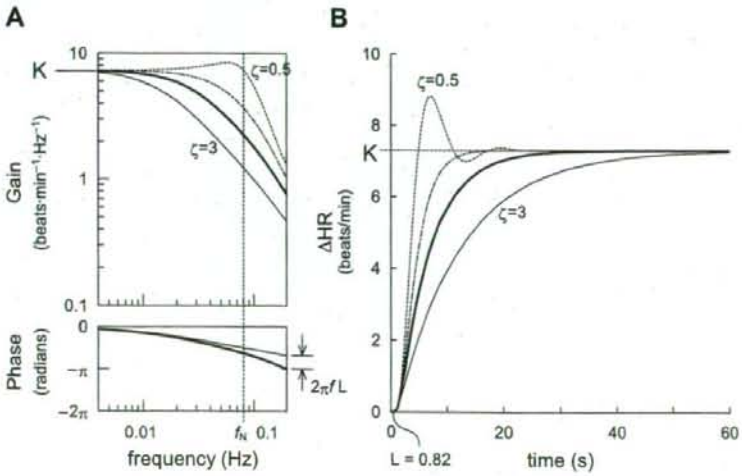

Fig. 7. Schematic explanation for the frequency response of a second-order, low-pass filter with pure dead time (*L*; *A*), and the corresponding step response (*B*). *K*, dynamic gain; f_N, natural frequency; ζ, damping ratio. See APPENDIX for details.

condition, the interpretation of the observed changes in the transfer function may be reasonable. Second, the simulation model in Fig. 6*A* is not the only model that can be applied to the observed results. Although the model is convenient to explain many aspects of the observed results, other models may also be applicable to the present observation. Third, clonidine can affect HR through non-α_2-adrenergic mechanisms. For instance, clonidine caused bradycardia in α_{2ABC}-knockout mouse via direct inhibition of cardiac hyperpolarization-activated cyclic nucleotide-gated pacemaker channels (16). While we tried to use medetomidine instead of clonidine, medetomidine did not attenuate myocardial interstitial NE release in response to sympathetic nerve stimulation significantly, at least, at the same dose as clonidine (Fig. 5). Further studies using other agonists might be required to confirm our observations. Finally, we used a weak stimulus rate (0 to 1 Hz) for the yohimbine protocol. Although we had examined the effect of yohimbine using a strong stimulus rate (0–5 Hz) in a preliminary study, the steady-state gain of the transfer function did not increase much (8.4 ± 1.7 vs. 9.0 ± 1.7 beats·min^{-1}·Hz^{-1}, $n = 3$). Under such strong stimulus condition, the saturation of HR response might have masked the effect of presynaptic inhibition. Therefore, the result of *protocol 1* should be carefully interpreted in view of the existence of a stimulus rate-drug interaction effect.

Conclusions

The presynaptic α_2-adrenergic autoinhibition attenuates the dynamic HR response to sympathetic nerve stimulation in the low-frequency range (0.004–0.04 Hz) but not in the high-frequency range (0.05–0.15 Hz). In the time domain, the presynaptic α_2-adrenergic autoinhibition attenuates the steady-state response without affecting the slope of the response in the HR step response (a limiter-like operation). In contrast, pharmacologic augmentation of presynaptic α_2-adrenergic inhibition attenuates the dynamic HR response to sympathetic nerve stimulation in a frequency-independent manner. In the time domain, pharmacologic augmentation of the presynaptic inhibition attenuates not only the steady-state response but also the initial slope of the HR step response (an attenuator-like operation). Presynaptic α_2-adrenergic autoinhibition would be favorable for limiting excess NE outflow at the sympathetic nerve terminals without compromising the rapidity of effector response.

APPENDIX

Mathematical Modeling of the Sympathetic HR Response

To describe the estimated transfer function, we used a second-order, low-pass filter with pure dead time (L). Figure 7*A* shows the frequency response of a second-order, low-pass filter with L. Figure 7*B* shows the corresponding step response. The step response is calculated for 1-Hz sympathetic nerve stimulation. The steady-state gain (K) of the transfer function represents the value of transfer gain as the frequency approaches zero. The K corresponds to the steady-state response in the step-response representation. The natural frequency (f_N) determines the upper frequency limit of the low-pass filter. For instance, if the f_N were 10 times higher, the frequency axis in Fig. 7*A* would have to be scaled by a factor of 10, indicating that the system could respond to 10-fold higher frequency input. The phase plot in Fig. 7*A* indicates that, at the f_N, the output is delayed by $\pi/2$ radians relative to the input, in the absence of the L. The maximum phase delay of the second-order, low-pass filter is π radians in the absence of L. The L is needed to account for the phase difference between the estimated transfer function and the second-order, low-pass filter. In Fig. 7*B*, the L corresponds to the time difference between the onset of the step input and the onset of the response. The damping coefficient (ζ) characterizes the system response around the f_N. As an example, the gain plot shows a slight peak around f_N when $\zeta = 0.5$ (dotted line). Figure 7*B* shows that a ζ of 0.5 causes an initial overshoot in response to a step change in the input. A system with $\zeta < 1$ is called underdamped. On the other hand, the gain plot shows more gradual decrease around f_N when $\zeta = 3$ (fine solid line). Figure 7*B* shows that the system responds sluggishly when $\zeta = 3$. A system with $\zeta > 1$ is called overdamped. A system with $\zeta = 1$ is called critically damped (dash-dot line). The ζ of the estimated transfer functions ranged from 1.55 to 1.72 in the present study, indicating that the sympathetic HR control system is overdamped. The solid line represents the second-order, low-pass filter with $\zeta = 1.64$ and $L = 0.82$ that is derived from the mean value obtained under control condition in *protocol 1*.

GRANTS

This study was supported by "Health and Labour Sciences Research Grant for Research on Advanced Medical Technology," "Health and Labour Sciences Research Grant for Research on Medical Devices for Analyzing, Supporting and Substituting the Function of Human Body," and "Health and Labour Sciences Research Grant H18-Iryo-Ippan-023" from the Ministry of Health, Labour and Welfare of Japan; "Program for Promotion of Fundamental Studies in Health Science" from the National Institute of Biomedical Innovation; and "Ground-based Research Announcement for Space Utilization" promoted by the Japan Space Forum.

REFERENCES

1. **Altman JD, Trendelenburg AU, MacMillan L, Bernstein D, Limbird L, Starke K, Kobilka BK, Hein L.** Abnormal regulation of the sympathetic nervous system in α_{2A}-adrenergic receptor knockout mice. *Mol Pharmacol* 56: 154–161, 1999.
2. **Bendat JS, Piersol AG.** Single-input/output relationships. In: *Random Data Analysis and Measurement Procedures* (3rd Ed.). New York: Wiley, 2000, p. 189–217.
3. **Berger RD, Saul JP, Cohen RJ.** Transfer function analysis of autonomic regulation. I. Canine atrial rate response. *Am J Physiol Heart Circ Physiol* 256: H142–H152, 1989.
5. **Brigham EO.** FFT transform applications. In: *The Fast Fourier Transform and Its Applications*. Englewood Cliffs, NJ: Prentice-Hall, 1988, p. 167–203.
6. **Buhler FR, Bolli P, Amann WF, Erne P, Kiowski W.** Sympathetic nervous system in essential hypertension and antihypertensive response to α_2-adrenoceptor stimulation. *J Cardiovasc Pharmacol* 6: S753–S756, 1984.
7. **Franklin GF, Powell JD, and Emani-Naeini A.** Dynamic models and dynamic response. In: *Feedback Control of Dynamic Systems* (2nd Ed.). Boston, MA: Addison-Wesley, 1991, p. 17–144.
8. **Glantz SA.** *Primer of Biostatistics* (5th Ed.). New York: McGraw-Hill, 2002.
9. **Grossman E, Chang PC, Hoffman A, Tamrat M, Goldstein DS.** Evidence for functional α_2-adrenoceptors on vascular sympathetic nerve endings in the human forearm. *Circ Res* 69: 887–897, 1991.
10. **Hein L, Altman JD, Kobilka BK.** Two functionally distinct α2-adrenergic receptors regulate sympathetic neurotransmission. *Nature* 402: 181–184, 1999.
11. **Jie K, van Brummelen P, Vermey P, Timmermans PB, van Zwieten PA.** Modulation of noradrenaline release by peripheral presynaptic α_2-adrenoceptors in humans. *J Cardiovasc Pharmacol* 9: 407–413, 1987.
12. **Kawada T, Ikeda Y, Sugimachi M, Shishido T, Kawaguchi O, Yamazaki T, Alexander J Jr, Sunagawa K.** Bidirectional augmentation of heart rate regulation by autonomic nervous system in rabbits. *Am J Physiol Heart Circ Physiol* 271: H288–H295, 1996.
13. **Kawada T, Sugimachi M, Shishido T, Miyano H, Sato T, Yoshimura R, Miyashita H, Nakahara T, Alexander J Jr, Sunagawa K.** Simultaneous identification of static and dynamic vagosympathetic interactions in regulating heart rate. *Am J Physiol Regul Integr Comp Physiol* 276: R782–R789, 1999.

14. **Kawada T, Yamazaki T, Akiyama T, Sato T, Shishido T, Sugimachi M, Inagaki M, Alexander J Jr, Sunagawa K.** Liquid chromatographic determination of myocardial interstitial epinephrine. *J Chromatogr B Biomed Sci Appl* 714: 375–378, 1998.
15. **Kawada T, Yamazaki T, Akiyama T, Sato T, Shishido T, Yoshimura R, Inagaki M, Tatewaki T, Sugimachi M, Sunagawa K.** Local epinephrine release in the rabbit myocardial interstitium in vivo. *J Auton Nerv Syst* 78: 94–98, 2000.
16. **Knaus A, Zong X, Beetz N, Jahns R, Lohse MJ, Biel M, Hein L.** Direct inhibition of cardiac hyperpolarization-activated cyclic nucleotide-gated pacemaker channels by clonidine. *Circulation* 115: 872–880, 2007.
17. **Langer SZ.** 25 years since the discovery of presynaptic receptors, present knowledge and future perspectives. *Trends Pharmacol Sci* 18: 95–99, 1997.
18. **Langer SZ.** Presence and physiological role of presynaptic inhibitory α_2-adrenoreceptors in guinea pig atria. *Nature* 294: 671–672, 1981.
19. **Langer SZ, Adler-Graschinsky E, Giorgi O.** Physiological significance of α-adrenoceptor-mediated negative feedback mechanism regulating noradrenaline release during nerve stimulation. *Nature* 265: 648–650, 1977.
20. **Langer SZ.** Presynaptic regulation of catecholamine release. *Biochem Pharmacol* 23: 1793–1800, 1974.
21. **Marmarelis PZ, Marmarelis VZ.** The white noise method in system identification. In: *Analysis of Physiological Systems*. New York: Plenum, 1978, p. 131–221.
22. **Miyamoto T, Kawada T, Yanagiya Y, Takaki H, Inagaki M, Sugimachi M, Sunagawa K.** Cardiac sympathetic nerve stimulation does not attenuate dynamic vagal control of heart rate via α-adrenergic mechanism. *Am J Physiol Heart Circ Physiol* 287: H860–H865, 2004.
23. **Nakahara T, Kawada T, Sugimachi M, Miyano H, Sato T, Shishido T, Yoshimura R, Miyashita H, Inagaki M, Alexander J Jr, Sunagawa K.** Neuronal uptake affects dynamic characteristics of heart rate response to sympathetic stimulation. *Am J Physiol Regul Integr Comp Physiol* 277: R140–R146, 1999.
24. **Niederhoffer N, Hein L, Starke K.** Modulation of the baroreceptor reflex by α_{2A}-adrenoceptors, a study in α_{2A} knockout mice. *Br J Pharmacol* 141: 851–859, 2004.
25. **Pelayo F, Dubocovich ML, Langer SZ.** Regulation of noradrenaline release in the rat pineal through a negative feedback mechanism mediated by presynaptic α-adrenoceptors. *Eur J Pharmacol* 45: 317–318, 1977.
26. **Philipp M, Brede M, Hein L.** Physiological significance of α_2-adrenergic receptor subtype diversity, one receptor is not enough. *Am J Physiol Regul Integr Comp Physiol* 283: R287–R295, 2002.
27. **Rump LC, Bohmann C, Schaible U, Schöllhorn J, Limberger N.** α2C-Adrenoceptor-modulated release of noradrenaline in human right atrium. *Br J Pharmacol* 116: 2617–2624, 1995.
27a. **Schwartz DD.** Activation of alpha-2 adrenergic receptors inhibits norepinephrine release by a pertussis toxin-insensitive pathway independent of changes in cytosolic calcium in cultured rat sympathetic neurons. *J Pharmacol Exp Ther* 282: 248–255, 1997.
28. **Sinclair MD.** A review of the physiological effects of α2-agonists related to the clinical use of medetomidine in small animal practice. *Can Vet J* 44: 885–897, 2003.
29. **Starke KM, Gothert M, Kilbinger H.** Modulation of neurotransmitter release by presynaptic autoreceptors. *Physiol Rev* 69: 864–989, 1989.
30. **Starke KM.** Presynaptic α-autoreceptors. *Rev Physiol Biochem Pharmacol* 107: 73–146, 1987.
31. **Starke K, Langer SZ.** A note on terminology for presynaptic receptors. In: *Presynaptic Receptors*, edited by Langer SZ, Starke K, and Dubocovich ML. Oxford, UK: Pergamon 1979, p. 1–3.
32. **Starke K, Endo T, Taube HD.** Pre- and post-synaptic components in effect of drugs with α-adrenoceptor affinity. *Nature* 254: 440–441, 1975.
33. **Starke K.** Alpha sympathomimetic inhibition of adrenergic and cholinergic transmission in the rabbit heart. *Naunyn Schmiedebergs Arch Pharmacol* 274: 18–45, 1972.
34. **Szabo B, Schramm A, Starke K.** Effect of yohimbine on renal sympathetic nerve activity and renal norepinephrine spillover in anesthetized rabbits. *J Pharmacol Exp Ther* 260: 780–788, 1992.
35. **Szabo B, Hedler L, Starke K.** Peripheral presynaptic and central effects of clonidine, yohimbine and rauwolscine on the sympathetic nervous system in rabbits. *Naunyn-Schmiedeberg's Arch Pharmacol* 340: 648–657, 1989.
37. **Vizi ES, Somogyi GT, Hadhazy P, Knoll J.** Effect of duration and frequency of stimulation on the presynaptic inhibition by α-adrenoceptor stimulation of the adrenergic transmission. *Naunyn-Schmiedeberg's Arch Pharmacol* 280: 79–91, 1973.
38. **Westfall TC.** Local regulation of adrenergic neurotransmission. *Physiol Rev* 57: 659–728, 1977.

Am J Physiol Heart Circ Physiol 295: H1081–H1089, 2008.
First published June 27, 2008; doi:10.1152/ajpheart.00023.2008.

Muscle mechanoreflex augments arterial baroreflex-mediated dynamic sympathetic response to carotid sinus pressure

Kenta Yamamoto,[1,2] Toru Kawada,[2] Atsunori Kamiya,[2] Hiroshi Takaki,[2] Toshiaki Shishido,[2] Kenji Sunagawa,[3] and Masaru Sugimachi[2]

[1]*Consolidated Research Institute for Advanced Science and Medical Care, Waseda University, Tokyo;* [2]*Department of Cardiovascular Dynamics, Advanced Medical Engineering Center, National Cardiovascular Center Research Institute, Osaka; and* [3]*Department of Cardiovascular Medicine, Graduate School of Medical Sciences, Kyushu University, Fukuoka, Japan*

Submitted 8 January 2008; accepted in final form 19 June 2008

Yamamoto K, Kawada T, Kamiya A, Takaki H, Shishido T, Sunagawa K, Sugimachi M. Muscle mechanoreflex augments arterial baroreflex-mediated dynamic sympathetic response to carotid sinus pressure. *Am J Physiol Heart Circ Physiol* 295: H1081–H1089, 2008. First published June 27, 2008; doi:10.1152/ajpheart.00023.2008.—Although the muscle mechanoreflex is one of the pressor reflexes during exercise, its interaction with dynamic characteristics of the arterial baroreflex remains to be quantitatively analyzed. In anesthetized, vagotomized, and aortic-denervated rabbits ($n = 7$), we randomly perturbed isolated carotid sinus pressure (CSP) using binary white noise while recording renal sympathetic nerve activity (SNA) and arterial pressure (AP). We estimated the transfer functions of the baroreflex neural arc (CSP to SNA) and peripheral arc (SNA to AP) under conditions of control and muscle stretch of the hindlimb (5 kg of tension). The muscle stretch increased the dynamic gain of the neural arc while maintaining the derivative characteristics [gain at 0.01 Hz: 1.0 ± 0.2 vs. 1.4 ± 0.6 arbitrary units (au)/mmHg, gain at 1 Hz: 1.7 ± 0.6 vs. 2.7 ± 1.4 au/mmHg; $P < 0.05$, control vs. stretch]. In contrast, muscle stretch did not affect the peripheral arc. In the time domain, muscle stretch augmented the steady-state response at 50 s (−1.1 ± 0.3 vs. −1.7 ± 0.7 au; $P < 0.05$, control vs. stretch) and negative peak response (−2.1 ± 0.5 vs. −3.1 ± 1.5 au; $P < 0.05$, control vs. stretch) in the SNA step response. A simulation experiment using the results indicated that the muscle mechanoreflex would accelerate the closed-loop AP regulation via the arterial baroreflex.

muscle stretch; transfer function; exercise pressor reflex; exercise; arterial pressure

THE ARTERIAL BAROREFLEX SYSTEM plays an important role in stabilizing arterial pressure (AP) during daily activity. Knowledge of the open-loop static and dynamic characteristics of the arterial baroreflex is essential for a systematic understanding of how the baroreflex system regulates AP. The static characteristics provide information on the operating point of the baroreflex system (19, 34, 48), whereas the dynamic characteristics determine the stability and quickness of the baroreflex system (14, 22, 23). Importantly, many previous studies showed that exercise resets the baroreflex function (3, 5, 6, 29, 30, 32, 35, 36, 40, 45, 47). However, only a few investigations focused on the dynamic characteristics of the arterial baroreflex during exercise (10, 36, 38, 57). The dynamic characteristics of the arterial baroreflex determine how quickly or slowly the system would response to baroreceptor pressure perturbations. Such information cannot be obtained from the static characteristics alone.

The neural mechanisms responsible for changes in the baroreflex function during exercise are considered to be mediated by central command (6, 13, 29, 39, 46) and by afferent inputs from metabolic and mechanical-sensitive skeletal muscle receptors (11, 12, 17, 41, 43, 44, 49). Regarding the static interaction between the muscle mechanoreflex and arterial baroreflex, we performed a baroreflex open-loop study and reported that muscle stretch extended the response range of sympathetic nerve activity (SNA) to baroreceptor pressure input (58, 59). Based on the results, we hypothesized that the activation of the muscle mechanoreflex would augment the dynamic SNA response to baroreceptor pressure input under open-loop conditions. To the best of our knowledge, however, the effects of the muscle mechanoreflex on the dynamic characteristics of the arterial baroreflex have never been reported.

To test the above hypothesis, we identified the dynamic characteristics of the baroreflex during muscle stretch in anesthetized rabbits under baroreflex open-loop conditions (14, 22, 23). The transfer functions from baroreceptor pressure input to SNA (the baroreflex neural arc) and from SNA to AP (the baroreflex peripheral arc) were estimated by a white noise approach (51). The "whiteness" is essential for the system identification of the arterial baroreflex because it is equivalent mathematically to test the system with all possible pressure changes within the frequency range of interest.

METHODS

Surgical preparations. Animals were cared for in strict accordance with the Guiding Principles for the Care and Use of Animals in the Field of Physiological Sciences approved by the Physiological Society of Japan. All protocols were approved by the Animal Subjects Committee of the National Cardiovascular Center. Seven Japanese White rabbits weighing 2.6–3.0 kg were anesthetized via an intravenous injection (2 ml/kg) of a mixture of urethane (250 mg/ml) and α-chloralose (40 mg/ml) and were mechanically ventilated with oxygen-enriched room air. Supplemental anesthetics (0.2–0.3 $ml \cdot kg^{-1} \cdot h^{-1}$) were administered continuously to maintain stable AP and heart rate levels during intervals of experimental protocols, which were indicative of an appropriate level of anesthesia. Arterial blood was sampled from the left common carotid artery. Rabbits were slightly hyperventilated to suppress chemoreflexes (arterial P_{CO_2} ranged from 30 to 35 mmHg, arterial $P_{O_2} > 300$ mmHg). Arterial blood pH was within the

Address for reprint requests and other correspondence: K. Yamamoto, Consolidated Research Institute for Advanced Science and Medical Care, Waseda Univ., 513 Wasedatsurumakicho, Shinjuku, Tokyo 162-0041, Japan (e-mail: kenta@aoni.waseda.jp).

The costs of publication of this article were defrayed in part by the payment of page charges. The article must therefore be hereby marked "*advertisement*" in accordance with 18 U.S.C. Section 1734 solely to indicate this fact.

physiological range when examined at the end of the surgical preparation as well as at the end of the experiment. The body temperature of each animal was maintained at ~38°C with a heating pad. AP was measured using a high-fidelity pressure transducer (Millar Instruments, Houston, TX) inserted from the right femoral artery to the aortic arch.

We isolated bilateral carotid sinuses from the systemic circulation by ligating the internal and external carotid arteries and other small branches originating from the carotid sinus region. Isolated carotid sinuses were filled with warmed physiological saline via catheters inserted through the common carotid arteries. Intra-CSP was controlled by a servo-controlled piston pump (model ET-126A, Labworks, Costa Mesa, CA). Bilateral vagal and aortic depressor nerves were sectioned at the neck to minimize reflexes from the cardiopulmonary region and from the aortic arch.

We exposed the left renal sympathetic nerve retroperitoneally and attached a pair of stainless steel wire electrodes (Bioflex wire AS633, Cooner Wire, Chatsworth, CA) to record SNA. The nerve bundle peripheral to the electrodes was tightly ligated and crushed to eliminate afferent signals from the kidney. The nerve and electrodes were secured with silicone glue (Kwik-Sil, World Precision Instruments, Sarasota, FL). The preamplified nerve signal was band-pass filtered at 150–1,000 Hz, full-wave rectified, and low-pass filtered with a cutoff frequency of 30 Hz to quantify the nerve activity.

With the rabbit in the prone position, the sacrum, left ankle, and knee were clamped with a custom-made apparatus to prevent body trunk and hindlimb movement during muscle stretch. The left triceps surae muscle, Achilles tendon, and calcaneus bone were exposed. The left triceps surae muscle was isolated from the surrounding tissue. The Achilles tendon was severed from the calcaneus bone and attached to a force transducer (Load Cell LUR-A-SA1, Kyowa Electronic Instruments, Tokyo, Japan). During muscle stretch, the other side of the force transducer was connected to a 5-kg weight via a pulley.

Protocols. To obtain operating pressure values, the carotid sinus baroreflex negative feedback loop was effectively closed by adjusting CSP to AP. Mean AP (and thus mean CSP) at steady state was treated as the operating pressure under control conditions. We then performed muscle stretch for 1 min while the carotid sinus baroreflex was effectively closed. Mean AP during the last 10 s of muscle stretch was treated as the operating pressure under muscle stretch conditions.

To estimate the baroreflex dynamic characteristics, CSP was assigned either high (+20 mmHg) or low (−20 mmHg) pressure values around the operating pressure according to a binary white noise sequence. The switching interval of the binary white noise signal was set at 500 ms so that the CSP power spectrum was fairly flat up to 1 Hz. We confirmed that the muscle stretch produced a sustained SNA increase for at least 7 min (58). To limit the maximum duration of muscle stretch within this time period, a 6-min CSP perturbation was performed twice using different binary sequences, and the two sets of data were pooled for analyses under both control and muscle stretch conditions. The order of control and muscle stretch conditions was randomized across the animals.

Data analysis. We recorded CSP, muscle tension, SNA, and AP at a sampling rate of 200 Hz using a 12-bit analog-to-digital converter. Data were stored on a dedicated laboratory computer system.

To estimate the neural arc transfer function of the carotid sinus baroreflex, we treated CSP as the input and SNA as the output of the system. In the peripheral arc transfer function, we treated SNA as the input and AP as the output of the system. In the total loop transfer function, we treated CSP as the input and AP as the output of the system. Data analysis was started from 90 s after the initiation of each trial to process the stationary portion of data without the effects of transition from closed-loop CSP waveform to open-loop binary white noise CSP input and the transition from nonstretch to stretch of muscle mechanoreceptors. The input-output data pairs were resampled at 10 Hz and segmented into 50%-overlapping bins of 1,024 points each. For each segment, a linear trend was subtracted, and a Hanning window was applied. A fast Fourier transform was performed to obtain the frequency spectra of the input and output signals. The ensemble averages of input power spectral density [$S_{XX}(f)$], output power spectral density [$S_{YY}(f)$], and cross-spectral density between the input and output [$S_{YX}(f)$] were obtained over eight segments derived from two sets of data, where f represents frequency. Finally, we calculated the transfer function from input to output [$H(f)$] using the following equation (27):

$$H(f) = \frac{S_{YX}(f)}{S_{XX}(f)} \quad (1)$$

Hereinafter, we denote the modulus as the dynamic gain of the transfer function. To quantify the linear dependence between input and output signals in the frequency domain, we calculated a magnitude-squared coherence function [Coh(f)] using the following equation (27):

$$\mathrm{Coh}(f) = \frac{|S_{YX}(f)|^2}{S_{XX}(f)S_{YY}(f)} \quad (2)$$

The coherence value ranges from zero to unity. Unity coherence indicates perfect linear dependence between input and output signals, whereas zero coherence indicates total independence between the two signals.

To facilitate an intuitive understanding of the transfer function, the step response corresponding to the transfer function was also calculated as follows. The system impulse response was derived from the inverse Fourier transform of $H(f)$. The step response was obtained from the time integral of the impulse response.

Statistical analysis. All data are presented as means ± SD. Because the amplitude of SNA varied depending on recording conditions, such as the physical contact between the nerve and electrodes, SNA was presented in arbitrary units (au). Neural and peripheral arc transfer functions were normalized in each animal so that the average gain values below 0.03 Hz in the control trial became unity. To compare the transfer functions between two conditions, a transfer gain value at 0.01 Hz ($G_{0.01}$), 0.1 Hz ($G_{0.1}$), 0.5 Hz ($G_{0.5}$), and 1 Hz (G_1) were calculated. In the step response of the neural arc, the steady-state step response at 50 s (S_{50}), the negative peak value (S_{peak}), and the time to negative peak (T_{peak}) were calculated. The effects of muscle stretch on these parameters were examined using the paired t-test. Differences were considered significant when $P < 0.05$.

RESULTS

Figure 1 shows a typical time series of CSP, muscle tension, SNA, and AP under control (*left*) and muscle stretch (*right*) conditions. Although the same binary sequence was applied for two conditions in each animal, different binary sequences were applied for different animals to reduce possible systematic errors in system identification caused by a bias in whiteness specific to a selected binary sequence. The mean CSP during muscle stretch conditions (Fig. 1, *right*) was set higher than that during the control conditions (Fig. 1, *left*) to mimic the increase in the operating pressure during muscle stretch under baroreflex closed-loop conditions (i.e., the AP increase by muscle stretch increases the mean input pressure to the baroreceptors) . Muscle stretch increased mean levels of SNA and AP compared with control conditions during the experiment (Table 1).

Figure 2 shows the transfer functions of the neural (*left*) and peripheral (*right*) arcs estimated under the control and muscle stretch conditions; gain plots (*top*), phase plots (*middle*), and Coh(f) (*bottom*) are also presented. The thin and thick solid lines in Fig. 2 indicate control and muscle stretch conditions, respectively. In the neural arc, the dynamic gain increased as

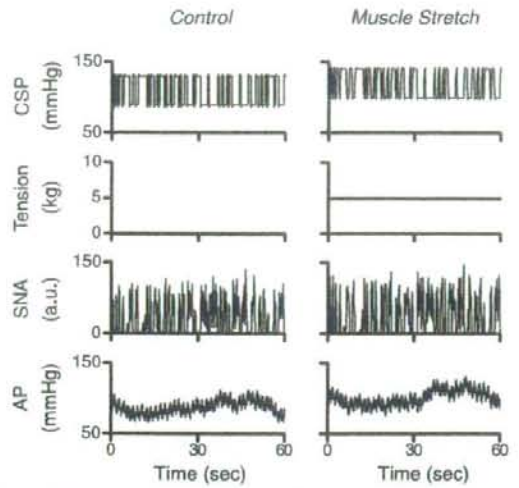

Fig. 1. Typical time series of intracarotid sinus pressure (CSP), muscle tension, sympathetic nerve activity [SNA; in arbitrary units (au)], and arterial pressure (AP) under control (*left*) and muscle stretch (*right*) conditions. CSP was perturbed according to a binary white noise sequence. Muscle stretch increased mean levels of SNA and AP under muscle stretch conditions compared with the control conditions.

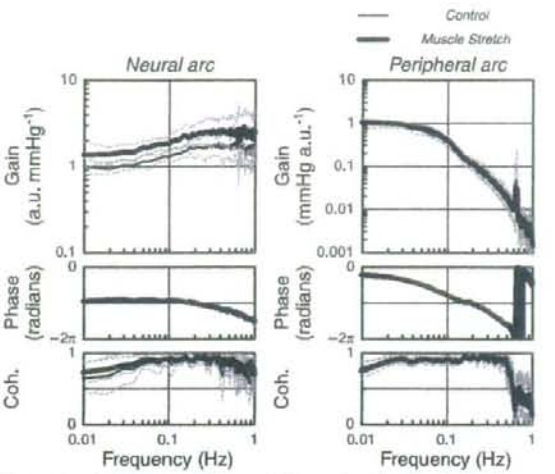

Fig. 2. Transfer functions of the neural (*left*) and peripheral (*right*) arcs under control and muscle stretch conditions. In the neural arc, the input was CSP and the output was SNA. In the peripheral arc, the input was SNA and the output was AP. The mean level of CSP input to the neural arc was set higher under muscle stretch conditions than under control conditions to mimic the physiological condition (i.e., baroreflex closed-loop conditions). Gain plots (*top*), phase plots (*middle*) and coherence (Coh) functions (*bottom*) are shown. Thin and thick solid lines indicate control and muscle stretch conditions, respectively. In the neural arc (*left*), muscle stretch caused an approximately parallel upward shift of the gain plot. Solid and dashed lines represent means and means ± SD values, respectively.

the frequency of input modulation increased under both conditions, indicating derivative characteristics of the neural arc. Muscle stretch caused an approximately parallel upward shift of the gain plot. The phase approached $-\pi$ radians ($-180°$) at the lowest frequency (0.01 Hz) under both conditions, reflecting the negative feedback character of the baroreflex neural arc (i.e., an increase in CSP decreased SNA). Phase plots were nearly superimposed between the two conditions. Coherence values did not differ between both conditions. In the peripheral arc, the dynamic gain decreased in the frequency range from 0.05 to 1 Hz as the frequency of input modulation increased under both conditions, indicating the low-pass characteristics of the peripheral arc. The phase approached 0 radians at the lowest frequency (0.01 Hz) under both conditions, reflecting the fact that an increase in SNA increased AP. The phase lagged with increasing frequency up to 1 Hz. The gain plot, phase plot, and Coh(*f*) did not differ between both conditions.

Table 2 summarizes gains of the transfer functions. In the neural arc, $G_{0.01}$, $G_{0.1}$, $G_{0.5}$, and G_1 were higher under muscle

Table 1. *Mean levels and CVs of CSP, SNA, and AP at 1, 2, 4, and 6 min under control and muscle stretch conditions*

	Time			
	1 min	2 min	4 min	6 min
		CSP		
Control	95±18	96±18	95±18	96±18
CV	13±2	12±3	11±3	14±2
Muscle stretch	114±15*	115±16*	113±16*	114±15*
CV	11±2	11±1	10±2	12±2
		SNA		
Control	102±4	99±5	100±4	99±4
CV	46±11	45±9	43±9	47±9
Muscle stretch	133±22*	129±21*	127±17*	126±17*
CV	48±11	47±8	44±9	49±10
		AP		
Control	90±21	89±20	88±16	88±18
CV	7±2	6±2	6±2	6±2
Muscle stretch	107±26*	105±22*	104±15*	101±15*
CV	7±3	6±3	6±3	7±2

Values are means ± SD; $n = 7$. CSP, carotid sinus pressure (in mmHg); SNA, sympathetic nerve activity (in %); AP, arterial pressure (in mmHg); CV, coefficient of variation. Mean and CV values were calculated from 30-s data ending at each time point. *$P < 0.05$ vs. control.

Table 2. *Gains of the transfer functions*

	Control	Muscle Stretch
Neural arc		
$G_{0.01}$, au/mmHg	1.01±0.23	1.44±0.56*
$G_{0.1}$, au/mmHg	1.30±0.11	1.86±0.37*
$G_{0.5}$, au/mmHg	1.77±0.64	2.65±1.08*
G_1, au/mmHg	1.72±0.66	2.72±1.40*
Peripheral arc		
$G_{0.01}$, mmHg/au	1.08±0.06	1.06±0.20
$G_{0.1}$, mmHg/au	0.37±0.09	0.42±0.09
$G_{0.5}$, mmHg/au	0.02±0.01	0.02±0.01
G_1, mmHg/au	0.004±0.001	0.004±0.002
Total loop		
$G_{0.01}$, mmHg/mmHg	1.08±0.18	1.53±0.63*
$G_{0.1}$, mmHg/mmHg	0.48±0.12	0.81±0.31*
$G_{0.5}$, mmHg/mmHg	0.04±0.04	0.06±0.04*
G_1, mmHg/mmHg	0.006±0.003	0.013±0.013

Values are means ± SD; $n = 7$. $G_{0.01}$, $G_{0.1}$, $G_{0.5}$, and G_1, dynamic gains at 0.01, 0.1, 0.5, and 1 Hz, respectively; au, arbitrary units. *$P < 0.05$ vs. control.

stretch compared with control conditions. In the peripheral arc, $G_{0.01}$, $G_{0.1}$, $G_{0.5}$, and G_1 were unchanged between control and muscle stretch conditions.

Figure 3 shows the total baroreflex loop transfer functions (CSP to AP) under control and muscle stretch conditions. The thin and thick solid lines in Fig. 3 indicate control and muscle stretch conditions, respectively. The dynamic gain decreased as the frequency of input modulation increased under both conditions, indicating low-pass characteristics. The dynamic gain under muscle stretch conditions was higher than that under control conditions in frequency from 0.01 to 0.5 Hz (Table 2). The phase plot and Coh(f) did not differ between both conditions.

Figure 4 shows step responses of SNA corresponding to the transfer functions in the neural arc shown in Fig. 2. The initial drop in the SNA response as well as the steady-state response was augmented during muscle stretch (Table 3). T_{peak} did not differ between control and muscle stretch conditions (Table 3).

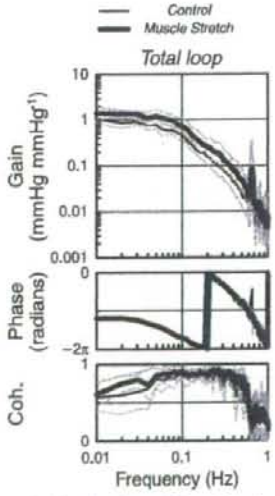

Fig. 3. Total loop transfer functions from CSP to AP under control and muscle stretch conditions. Gain plots (*top*), phase plots (*middle*) and coherence functions (*bottom*) are shown. Thin and thick solid lines indicate control and muscle stretch conditions, respectively. The dynamic gain decreased as the frequency of input modulation increased under both conditions, indicating low-pass characteristics. Muscle stretch caused an approximately parallel upward shift of the gain plot. Solid and dashed lines represent means and means ± SD values, respectively.

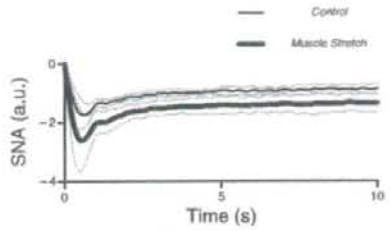

Fig. 4. Step responses corresponding to transfer functions of the neural arc obtained from Fig. 2, showing the SNA response to a 1-mmHg increase in input pressure. Thin and thick solid lines indicate control and muscle stretch conditions, respectively. The initial drop in the SNA response as well as the steady-state response was augmented by the muscle stretch. Solid and dashed lines represent means and means ± SD values, respectively.

DISCUSSION

The key new findings of the present study are as follows. Muscle stretch increased the dynamic gain of the carotid sinus baroreflex neural arc as estimated by binary white noise input (Fig. 2). In contrast, the peripheral arc transfer function remained unchanged irrespective of the muscle stretch (Fig. 2). These results suggest that during muscle mechanoreflex activation, the dynamic SNA response to CSP perturbation is augmented.

System identification by the white noise approach. To identify the dynamic characteristics of arterial baroreflex function quantitatively, we described the carotid sinus baroreflex control of SNA and AP in terms of system identification using the white noise technique. Compared with the traditional approach of testing dynamic properties of the physiological system with step and sine wave stimuli, the white noise approach has definite advantages, as follows (27). First, if a step stimulus is applied, we learn the response of the system to this step and have little notion of the response of the system to any other type of stimulus. If a sinusoidal pulse is applied, then we know the response of the system to such a stimulus and little else. The same applies for any other specific waveform. Theoretically speaking, the system is tested with every possible stimulus in the white noise approach. The white noise stimulus is a very rich stimulus. It should be emphasized that the white noise method is perfectly suited to the analysis of linear systems. As shown in Figs. 2 and 3, high coherence values close to unity indicate the validity of our method for system identification. Second, the identification of the physiological system through the white noise technique is largely unaffected by the types of contaminating noise usually present in such a system. Our study provides the first and quantitative description of the dynamic characteristics of the carotid sinus baroreflex during isolated activation of mechanosensitive afferents from skeletal muscle.

Effects of the muscle mechanoreflex on dynamic characteristics of the carotid sinus baroreflex. The effects of activation of afferents from skeletal muscle, such as those occurring during exercise, on the arterial baroreflex have been extensively studied (5, 13, 29, 42, 43, 49, 58, 59). These studies have demonstrated that the afferent input from muscle resets the baroreflex control of AP, heart rate, and SNA. However, the dynamic characteristics of the arterial baroreflex during isolated activation of muscle mechanosensitive afferents have never been analyzed. In the present study, muscle stretch increased dynamic gain in every frequency (Fig. 2 and Table

Table 3. *Parameters of step responses*

	Control	Muscle Stretch
S_{50}, au	−1.05±0.30	−1.69±0.69*
S_{peak}, au	−2.10±0.50	−3.08±1.45*
T_{peak}, s	0.63±0.21	0.64±0.20

Values are means ± SD; n = 7. A step response is defined as a SNA response to a 1-mmHg change in input pressure. S_{50}, step response at 50 s; S_{peak}, negative peak response; T_{peak}, time to negative peak. *P < 0.05 vs. control.

2), whereas it did not affect the peripheral arc. These data are the first to provide quantitative evidence demonstrating that the dynamic SNA response to CSP perturbation is augmented during isolated activation of the muscle mechanoreflex. Although an increase in dynamic gain in the lowest frequency (0.01 Hz) was expected from the results of our previous studies showing an increase in static gain by muscle stretch (58, 59), the information was insufficient to perform a simulation study to examine the effects of muscle stretch on the closed-loop dynamic AP regulation (see *Physiological implications*). The present study extended our previous work by providing additional information on the dynamic interaction over a wide range of frequencies between 0.01 and 1 Hz in the carotid sinus baroreflex.

The static characteristics of the arterial baroreflex determine an operating point of the baroreflex system. Furthermore, the static characteristics described by a modeled sigmoid function provide the parameters of threshold, saturation, and maximal gain at the centering point. However, the static characteristics alone cannot provide the information on the changes over time in the response of the baroreflex system. On the other hand, dynamic analysis techniques such as transfer function analysis estimated by the white noise approach provide information on the stability and quickness of the system response. The dynamic SNA response to baroreceptor pressure input became greater as the frequency of input modulation increased, suggesting derivative characteristics (i.e., high-pass characteristics) of the baroreflex neural arc (Fig. 2, *left*, thin solid line). In contrast, the dynamic AP response to SNA became smaller as the frequency of SNA modulation increased, indicating low-pass characteristics of the baroreflex peripheral arc (Fig. 2, *right*, thin solid line). The total loop transfer function (CSP to AP) is determined by a product of the neural and peripheral arc transfer functions (Fig. 3, thin solid line). Therefore, the decreasing slope of dynamic gain in the total loop transfer function was shallower than that in the corresponding peripheral arc. In other words, the fast neural arc effectively compensates for the slow peripheral arc to accelerate dynamic AP regulation by the baroreflex negative-feedback loop (14). During muscle stretch, the dynamic gain in the neural arc was increased by ~50% in every frequency under study (Fig. 2 and Table 2), indicating that the derivative characteristics of the neural arc were maintained. As a result, the effect of the neural arc compensating for the slow AP response was preserved during the activation of muscle mechanoreflex (Fig. 3 and Table 2). Furthermore, the total loop dynamic gain was augmented during the muscle stretch due to the upward shift of the neural arc transfer function.

Because we used passive muscle stretch as the input for the muscle mechanoreflex, the physiological significance of the present results should be interpreted carefully. Several studies have examined the arterial baroreflex control of SNA during static and dynamic exercise. Static and heavy dynamic exercise resets the baroreflex control of SNA to higher SNA levels with an increase in its sensitivity (9, 11, 17, 32). On the other hand, mild to moderate dynamic exercise resets the baroreflex control of SNA without any change in its sensitivity (3, 24, 38). Because the muscle mechanoreflex is activated during mild to moderate dynamic exercise (4), our results indicate that the muscle mechanoreflex may contribute to increasing the baroreflex gain of SNA during mild to moderate dynamic exercise. In addition to differences in the measured SNA (renal vs. muscle), analytic methods of baroreflex function, modes of mechanoreflex activation, and/or species between the present study and previous studies, the cardiopulmonary baroreflex should be taken into account. Charkoudian et al. (1) demonstrated that increasing central venous pressure via head-down tilt or saline infusion attenuated the baroreflex sensitivity in the control of SNA. The activation of cardiopulmonary baroreceptors induced by increasing central venous pressure may influence the arterial baroreflex control during dynamic exercise (37). In the present study, however, the cardiopulmonary baroreflex did not operate due to bilateral vagotomy.

Previous studies (7, 25) have suggested that the muscle mechanoreflex has a dominant role in pressor reflexes during muscle contraction in anesthetized or decerebrate cats. Although we believe that the mechanoreflex is one of the pressor reflexes during exercise, the functional importance of the muscle mechanoreflex in cardiovascular regulation during exercise in conscious conditions is debatable. Matsukawa et al. (28) recently reported that blockade of the muscle mechanoreflex by gadolinium did not alter AP responses to isometric exercise in conscious cats. Moreover, they found that gadolinium significantly diminished the pressor responses to passive muscle stretch in anesthetized cats. These observations suggest that, under the experimental design, the muscle mechanoreflex would not be activated during exercise or, even if it was activated, it has no functional importance in cardiovascular responses to exercise in conscious conditions. One criticism for the study is that there is always a possibility that changes in the central command in conscious conditions had compensated for the lack of muscle mechanoreflex. Further studies are needed to better understand the role of the muscle mechanoreflex on neural cardiovascular responses during exercise.

High-pass characteristics of the baroreflex neural arc. It is likely that the dynamic characteristics of the baroreflex neural arc actually reflect the intrinsic and synaptic properties of central nervous system neurons and neural circuits that transmit baroreceptor input. However, the central baroreceptor synapses are characterized as a low-pass filter (26). The difference between high-pass characteristics of the neural arc transfer gain and low-pass characteristics of the central baroreceptor synaptic transmission could be attributable to the difference of estimated frequency ranges. Frequency-dependent depression (FFD) of synaptic transmission in the baroreflex central pathways is the phenomenon that the probability of excitatory postsynaptic potentials progressively reduces as the frequency of afferent input increases beyond 1 Hz (2, 33). Although FDD and transfer gain should be discriminated in theory, interactions between FDD and transfer gain may occur when the modulation frequency of afferent fiber stimulation approached the frequency range of FDD. Indeed, Kawada et al. (23) found high-cut characteristics of the baroreflex neural arc in the frequency range above ~1 Hz. In the present study, the transfer gain was derived from 0.01 to 1 Hz. Whether the dynamic interaction between carotid sinus baroreflex and muscle mechanoreflex exists in the frequency range beyond 1 Hz awaits further studies.

Part of the high-pass characteristics in the baroreflex neural arc is attributable to the derivative nature observed in the baroreceptor transduction from CSP input to baroreceptor afferent nerve activity (i.e., mechanoneural transduction) (21).

However, we think there exists high-pass characteristics in the transduction from baroreceptor afferent input to efferent SNA, because the magnitude of high-pass characteristics slightly differs between cardiac and renal SNAs in response to the same baroreceptor pressure perturbation (18).

In an electrical circuit, we can design a high-pass filter only from low-pass filter elements using a feedback loop (Fig. 5). Although the main forward path of the baroreflex neural arc from afferent nerve activity to efferent SNA is considered to be the nucleus tructus solitarius, caudal ventrolateral medulla, and rostral ventrolateral medulla (53), there could be feedback connections between these areas. Therefore, it is possible that synaptic connection has basically low-pass characteristics, whereas the baroreflex neural arc reveals high-pass characteristics as a neural circuit. The speculation also needs to be verified experimentally in the future.

Physiological implications. Under physiological conditions, the baroreflex is closed as a negative feedback system. In the following discussion, we will focus on the effect of the augmentation of dynamic SNA modulation in the neural arc on the closed-loop dynamic AP regulation. Figure 6*A* illustrates a simulator consisting of the linear neural arc transfer function (H_N) and linear peripheral arc transfer function (H_P) followed by the nonlinear sigmoidal components (see the APPENDIX for details). A closed-loop AP response to a stepwise pressure perturbation (−40 mmHg) with pulsatile pressure was simulated, and the result is shown in Fig. 6*B*. Muscle stretch shortened the time to 95% of steady state by ~33% from 7.2 to 4.8 s (shaded and solid arrows in Fig. 6*B*). This result suggests that, under baroreflex closed-loop conditions, the rate of recovery in AP following a pressure perturbation occurs sooner when accompanied by the muscle mechanoreflex. Increasing the quickness of the negative-feedback system can be caused by augmentation and/or acceleration of the open-loop transfer function of the system. In our baroreflex open-loop experiment, S_{50} and S_{peak} in the step responses of SNA were augmented by the muscle stretch (Fig. 4 and Table 3). On the other hand, T_{peak} did not differ between control and muscle stretch conditions (Fig. 4 and Table 3). These results suggest that the improvement in the quickness of the AP restoration via the baroreflex observed in the closed-loop simulation was induced by augmentation, rather than acceleration, of the dynamic SNA response in the neural arc. However, further experimental studies are needed to verify the simulation model.

Limitations. The present study has several limitations. First, we performed the experiment in anesthetized animals. Previous studies have suggested that any anesthetic could alter the baroreflex regulation in AP (54–56). The gain of the baroreflex is reported in the conscious state to be higher (~2-fold) than in the anesthetized state. A previous study (52) suggested that α-chloralose anesthesia could alter the dynamic characteristics of the baroreflex regulation around the frequency of 5 Hz. However, the anesthesia was convenient for the elimination of the central command. Furthermore, we compared the baroreflex gain between muscle stretch and nonstretch conditions both under anesthesia. Therefore, a reasonable interpretation would be that the increased baroreflex gain is attributable to muscle stretch in this experiment.

Second, stretching of skeletal muscle provides a stimulus for the activation of mechanoreceptors that is different from that which occurs during muscle contraction. During contraction, mechanoreceptors are activated by a shortening of skeletal muscle and by compression of the receptors. Thus, mechanoreceptors may be stimulated in a very different manner during stretch, which would likely affect the magnitude of the corresponding reflex response. In addition, the level of muscle stretch used in our experiment was relatively high (50). The stretch may activate different afferents than contraction (8). Furthermore, the discharge profile of mechanosensitive afferents adapt during static muscle stretch (31). Accordingly, during the muscle stretch for 6 min in the present study, the firing level from the mechanoreceptors might have been

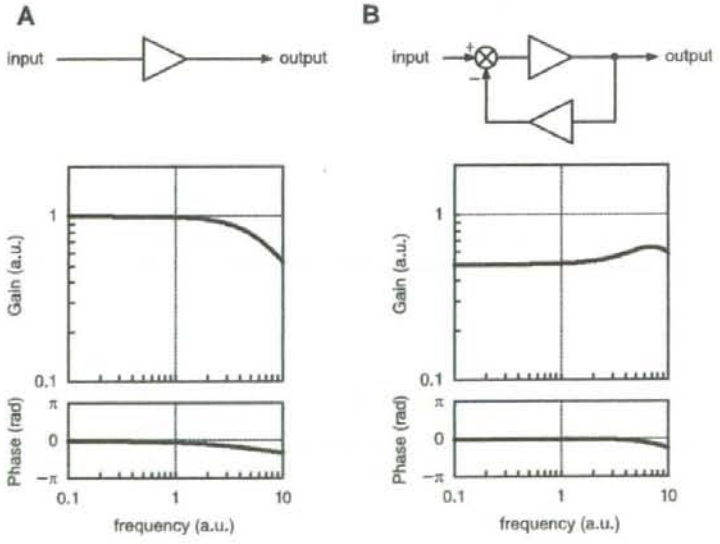

Fig. 5. An example that a circuit consisting of only low-pass elements yields high-pass characteristics as a circuit. *A*: block diagram of a single low-pass element (triangle) and its transfer function. Units for gain and frequency are arbitrary. *B*: block diagram of a circuit with a negative feedback loop with the same low-pass element (triangles). Because gain in the lower frequency range is attenuated more by the low-pass characteristics of the feedback path, the transfer function from input to output reveals high-pass characteristics.